Fiber-reinforced Viscoelastomers Show Extraordinary Crack Resistance that Exceeds Metals

*Wei Cui, Daniel R. King, Yiwan Huang, Liang Chen, Tao Lin Sun, Yunzhou Guo, Yoshiyuki Saruwatari, Chung-Yuen Hui, Takayuki Kurokawa, and Jian Ping Gong**

W. Cui, L. Chen, Y. Guo
Graduate School of Life Science, Hokkaido University, Sapporo 001-0021, Japan

Dr. D. R. King, Dr. Y. Huang, Dr. T. L. Sun, Prof. T. Kurokawa, Prof. J. P. Gong
Faculty of Advanced Life Science, Hokkaido University, Sapporo 001-0021, Japan
Email: gong@sci.hokudai.ac.jp

Dr. D. R. King, Prof. C. Y. Hui, Prof. T. Kurokawa, Prof. J. P. Gong
Global Station for Soft Matter, Global Institution for Collaborative Research and Education (GI-CoRE), Hokkaido University, Sapporo 001-0021, Japan

Dr. T. L. Sun
South China Advanced Institute for Soft Matter Science and Technology, South China University of Technology, Guangzhou, 510641, China

Dr. Y. Saruwatari
Osaka Organic Chemical Industry Ltd., Osaka, 541-0052, Japan

Prof. C. Y. Hui
Field of Theoretical & Applied Mechanics, Dept. of Mechanical & Aerospace Engineering, Cornell University, Ithaca, NY 14853, USA

Prof. J. P. Gong
Institute for Chemical Reaction Design and Discovery (WPI-ICReDD), Hokkaido University, Sapporo 001-0021, Japan.

Keywords: soft fiber-reinforced polymers, crack resistance, modulus ratio, force transfer length, energy dissipation density

Abstract

Soft fiber-reinforced polymers (FRPs), consisting of rubbery matrices and rigid fabrics, are widely utilized in industry because they possess high specific strength in tension while allowing flexural deformation under bending or twisting. Nevertheless, existing soft FRPs are relatively weak against crack propagation due to interfacial delamination, which substantially increases their risk of failure during use. In this work, a class of soft FRPs that possess high specific strength while simultaneously showing extraordinary crack resistance are developed. The strategy is to synthesize tough viscoelastic matrices from acrylate monomers in the presence of woven fabrics, which generates soft composites with a strong interface and interlocking structure. Such composites exhibit fracture energy, Γ, of up to 2500 kJ m^{-2}, exceeding the toughest existing materials. Experimental elucidation shows that the fracture energy obeys a simple relation, $\Gamma = W \cdot l_T$, where W is the volume-weighted average of work of extension at fracture of the two components and l_T is the force transfer length that scales with the square root of fiber/matrix modulus ratio. Superior Γ is achieved through a combination of extraordinarily large l_T (10~100 mm), resulting from the extremely high fiber/matrix modulus ratios (10^4~10^5), and the maximized energy dissipation density, W. The elucidated quantitative relationship provides guidance toward the design of extremely tough soft composites.

Many industrial applications require anisotropic structural materials that can bear considerable load in tension while showing flexibility when bent or twisted. Soft fiber-reinforced polymers (FRPs), consisting of soft, rubbery matrices and rigid fabrics, featuring high strength, high contact compliance, low weight and low flexural stiffness, are uniquely qualified for wide use such as in tires, conveyor belts, soft robotics, etc.[1-3] However, a common problem of soft FRPs made from conventional rubbery matrices is their relatively low crack resistance,[4, 5] which consequently results in increased risk of disastrous failure during their lifespan.

The crack resistance of a material is characterized by fracture energy, Γ, the energy required to create unit surface area for crack growth.[6-9] Simply, for tough materials, Γ is influenced by two factors: 1) the length over which a material is deformed inelastically ahead of the advancing crack, known as the energy dissipation zone size, l_T, and 2) the energy dissipation density of the dissipation zone when the crack advances, W. Accordingly, Γ (J m^{-2}) could be related to l_T (m) and W (J m^{-3}) by (**Figure 1**a),[10, 11]

$$\Gamma = W \cdot l_T \quad (1),$$

Therefore, developing tough materials is a question of how to design structures that maximize W and l_T. For composites consisting of a hard phase embedded in a soft matrix, assuming perfect interfacial bonding, W should result from the contributions of both components, so highly energy-dissipative components are preferred. On the other hand, l_T is related to the force transfer length, which depends on the mechanical properties and geometrical arrangement of the two components. For fiber-reinforced composites with strong interface, l_T scales with the square root of component modulus ratio (hard to soft).[12-14] For the combination of stiff fibers and conventional elastomers, this modulus ratio could be as high as 10^3~10^4, much higher than that ($<10^2$) of hard FRPs where the matrix materials are thermosetting plastics. Theoretically, soft FRPs can have very large l_T in comparison with the hard FRPs, which contributes to a high fracture energy, Γ. However, existing soft FRPs made from woven fabrics and rubbers cannot reach the theoretical value of l_T due to interfacial delamination.[15-17] Easy delamination at a

relatively small stress might also lead to small energy dissipation, which reduces W in Equation (1).[18, 19] These factors may account for the low crack growth resistance of existing soft FRPs.

Our strategy to enhance the crack resistance of soft FRPs is to employ viscoelastic polymer matrices that are adhesive, soft, and tough. These properties should not only enable a strong interface with the stiff reinforcing fibers, but also result in large force transfer lengths through high fiber/matrix modulus ratios, which contribute to a high energy dissipation density (W) and large energy dissipation zone (l_T). This tough viscoelastic matrix effect has recently been observed in fiber-reinforced hydrogel composites made from a polyampholyte (PA) hydrogel matrix and woven glass fiber fabric (GF).[20-22] The soft, de-swelled, and viscoelastic PA gel, with multiple ionic bonds in the network,[23] exhibits a strong adhesion to the negatively charged GF.[24] The fiber/matrix modulus ratio in this composite system is roughly 10^3 to 10^4, giving a force transfer length on the order of the cm-scale. As a result, the PA/GF composites, with highly energy-dissipative components and a large force transfer length, possess high tearing toughness while maintaining high tensile strength. However, such hydrogel-based soft composites cannot be used in ambient conditions since the inevitable water evaporation during use seriously deteriorates their mechanical performance and lifespan. Moreover, at this point in time there is little understanding of what controls the two important parameters, W and l_T of soft composites with a non-linear, viscoelastic matrix.

In this work, we develop tough, soft FRPs made of water-free viscoelastic matrices having a wide range of elastic modulus, and systematically study the crack resistance of these composites. Existing soft elastomers, such as polydimethylsiloxane, polyurethane, and natural rubber, can be combined with different fibers, but they do not satisfy the requirements of being simultaneously adhesive, soft, and tough. Therefore, we employ a class of newly developed "viscoelastomers" to fabricate a series of soft FRPs by combination with various woven fabrics. The viscoelastomer matrices are formed by one step radical copolymerization from liquid acrylate monomers without using solvent.[25] The low viscosity and good wettability of the

monomers to fiber surfaces of varying chemistry result in well-formed composites with strong fiber/matrix interface and interlocking structure. By changing the chemistry and the composition of the viscoelastomers, we tune the mechanical properties of the matrix over a wide range, and systematically study the quantitative relationship between the fracture energy of soft FRPs and the component material properties. We experimentally elucidate that 1) the energy dissipation density, W, in Equation (1) is related to the volume-weighted average of work of extension at fracture of the viscoelastomer and the fiber bundles, W_{eff}, and 2) the size of the energy dissipation zone, l_T, is proportional to the square root of the fiber/matrix modulus ratio, $l_T \sim (\frac{E_f}{\mu_m})^{\frac{1}{2}}$, at the condition of no interfacial delamination, where E_f and μ_m are the Young's modulus of the fiber and shear modulus of the matrix, respectively. As W_{eff} is the maximum energy density that could be dissipated, this result indicates that our soft FRPs take full advantage of the energy dissipation density in the dissipation zone, owing to the high toughness of the matrices along with the strong interface and interlocking structure.

Our findings show that a combination of high-strength, stiff fibers and adhesive, soft, tough viscoelastomers maximizes W and l_T and consequently enhances the toughness (Γ). By using specifically formulated viscoelastomers and aramid fiber fabrics, soft FRPs with extraordinarily high Γ of up to 2500 kJ m^{-2} are developed for the first time. The toughness is far superior to any best-in-class tough materials. The soft FRPs also show high strength (700 MPa) as well as low density (≈ 1 g cm^{-3}), comparable to traditional soft FRPs. This work provides a clear strategy for developing robust and lightweight soft FRPs for structural applications.

The geometry and mechanical properties of fabrics used in this work are given in Figure S1, Figure S2, and summarized in Table S1, Table S2 (Supporting Information). The viscoelastic matrices are synthesized from various pairs of acrylate monomers. In each pair of monomers, one acts as a soft segment and the other as a hard segment. Basic physicochemical properties of monomers used in this work are summarized in Table S3 (Supporting Information). As a

typical example, we first show soft FRPs fabricated from carbon fiber (CF) fabric and viscoelastomers P(PEA-*co*-IBA). The viscoelastomer matrix P(PEA-*co*-IBA), also denoted as M1-*f* (Figure 1b), is formed by UV-initiated free-radical copolymerization of the bulk monomers PEA (soft segment) and IBA (hard segment) in the presence of a small amount of benzophenone (BP) as initiator.[25] By varying the molar fraction of IBA, f ($f = \frac{M_{IBA}}{M_{IBA}+M_{PEA}}$) from 0.1 to 0.3, the T_g of the copolymers is tuned from 5 to 22 °C (Table S4). The materials show viscoelastic properties at room temperature (24 °C), and can be tuned over a wide range depending on the relative distance to their T_g (Figure 1c, Figure S4 and Table S5, Supporting Information) and the deformation rate.[25] Adhesion tests of a single fiber bundle partially embedded in M1-*f* matrix show that the fiber bundle outside the matrix breaks at a force of about 130 N for all tested matrices (Figure 1d), rather than being pulled out (Figure 1e). This result demonstrates that the interface and matrix do not fail, and the shear bonding strength (τ_s) of the interface should be higher than 2.28 MPa that is estimated by balancing the external force (F = 130 N) with the adhesion force provided by the shear bonding strength, as $F = \tau_s \cdot A$, where A is the embedded surface area of the fiber bundle. The bonding strength can be determined by decreasing the embedded length of the fiber bundle in the matrix to a critical length at which a transition from fiber fracture to fiber pullout occurs.[26, 27] As an example, the interfacial bonding strength between M1-0.2 matrix and a carbon fiber bundle was determined to be 11.9 MPa, higher than the fracture strength of the matrix (2.2 MPa) (Figure S5, Supporting Information). The strong adhesion should be attributed to Van der Waals interaction between fiber and matrix.

The soft FRP from M1-0.1 and CF is produced via a one-step random radical copolymerization of monomers in a mold where the fabric is sandwiched in the middle (Figure S6a, Supporting Information). The monomer is a low viscosity, hydrophobic, and non-volatile liquid at room temperature (Table S3, Supporting Information), which can wet the CF fabric and permeate easily into fiber bundles during monomer injection. As a result, the fabricated

composites have an interlocking structure between the two components, with the matrix strongly bonded to the fibers, as seen by SEM observation (Figure S6b, Supporting Information). The fabric can be seen in the soft FRP due to the optical transparency of the viscoelastomer matrix, and it is extremely resistant to stretching yet highly flexible to bending or twisting (**Figure 2**a).

Tensile tests and three-point bending tests reveal that the soft composite has a tensile modulus three orders of magnitude higher than the bending modulus (Figure S7, Supporting Information), due to the fabric phase lying nominally along the neutral axis during bending. Moreover, the soft FRP demonstrates an incredibly high crack resistance. A soft FRP sample (w = 80 mm) with two long precut cracks (30 mm) can hold 35 kg of hanging mass without crack propagation (Figure 2b).

Uniaxial tensile tests are conducted to measure the load-bearing properties. Sample geometries and corresponding stress-strain curves are shown in Figure 2c. The matrix is soft and highly stretchable, sustaining merely 1.5 MPa prior to failure with a work of extension of 6 MJ m^{-3} (inset of Figure 2c). On the contrary, the neat carbon fiber fabric is very stiff and strong (490 MPa) but brittle, failing at a strain of 8.8% and having a work of extension of 20 MJ m^{-3}. Interestingly, when the fabric is integrated with the matrix, the resulting composite shows a similar stiffness to the neat fabric, but it is much stronger (700 MPa) and breaks at a higher strain (12.5 %) than the neat fabric. The enhanced tensile behavior of soft FRPs compared to neat fabrics can be understood by a mechanism proposed by Hui et al, which highlights the role of modulus contrast.[14] The extremely large fiber/matrix modulus ratio means that the soft matrix can effectively transfer the lost load of the broken fiber to neighboring fibers by dramatically deforming in shear, resulting in a considerable overload region. Therefore, the lost load is carried by a broad region of adjacent fiber segments instead of being concentrated on a limited length scale, which delays the catastrophic failure of fibers.

Trouser tearing tests are performed to quantitatively measure the crack resistance of the

material (Methods, Supporting Information).[20-22, 28-30] As shown in Figure 2d, the composite achieves an extraordinarily high tearing force, which reaches a maximum value of 940 N mm^{-1}, much higher than 3.7 N mm^{-1} of the neat fabric and 13.3 N mm^{-1} of the neat matrix. The composite has a tearing toughness (T) as high as 1400 kJ m^{-2}, which is several orders of magnitude greater than both individual neat components (3.0 kJ m^{-2} for the neat fabric and 9.5 kJ m^{-2} for the neat matrix). The toughness of this composite is also much higher than any of the current best-in-class materials.[31-36]

Images of the composite after tearing reveals that the matrix is severely deformed over an area with a maximum dimension of several centimeters, indicating that both the matrix and fibers dissipate energy in a huge area ahead of the crack tip (Figure S8a, Supporting Information). A close SEM observation of the fractured surface further reveals that fibers break with no apparent interfacial debonding with the matrix (Figure S8b, Supporting Information). This fracture behavior notably contrasts with that of conventional soft FRPs fabricated from polymers and fabrics, which we also test for comparison. As shown in Figure S9 (Supporting Information), for the composites made from PDMS-based polymers and CF fiber, the interface fails before matrix rupture and fiber breaking, resulting in relatively low fracture energy. The weak interfacial strength for these composites is largely due to the high viscosity of polymers, which prevents good wetting of the polymers to the fabric during preparation. For the soft FRPs developed in this work, the low-viscosity monomer solution permeates fiber bundles entirely during preparation, forming interlocking structures after polymerization in addition to a good interface, which can effectively transfer the force by large shear deformation of soft matrix. This benefits the energy dissipation of the soft FRPs in three ways. First, the applied force can be transferred extensively through the composite, giving rise to a considerably large energy dissipation zone. Second, the tough matrix itself in the energy dissipation zone can dissipate large amounts of energy. Third, fibers in the energy dissipation zone are broken instead of being pulled out by debonding, which maximizes the elastic energy that the fibers can store and

dissipate. Endowed with large energy dissipation density and energy dissipation zone, the soft FRP possesses extraordinarily high fracture energy.

To reveal, quantitatively, the correlation between the mechanical properties of the viscoelastic matrices and the crack resistance of the soft FRPs, we further compare the behavior of soft FRPs by varying the mechanical properties of the matrix, P(PEA-*co*-IBA), by tuning *f*. The M1-0.3 viscoelastomer demonstrates relatively high modulus, fracture stress, work of extension, and tearing toughness when compared to M1-0.1 (Figure 1c, Figure S4, Supporting Information). The fiber/matrix modulus ratio (E_f/μ_m) of the f=0.3 composite is approximately 1.5×10^4, while the f=0.1 composite approaches 8.0×10^4. The force-displacement curves of the tearing tests are compared in **Figure 3**a. Both composites are sufficiently large (w =70 mm) to ensure that there is no size-dependent effect and the failure behavior is primarily fiber fracture. Interestingly, the f=0.1 composite with high E_f/μ_m is much more crack-resistant than the f=0.3 composite with low E_f/μ_m even though the former has a softer, weaker, and less tough matrix. The f=0.1 composite exhibits a much higher tearing force, which brings about a tearing toughness of 1400 kJ m^{-2}, outperforming the f=0.3 composite (550 kJ m^{-2}) by 150%.

Inset images in Figure 3a show the composites after tearing. In clear contrast with the limited distortion of the f=0.3 composite ($E_f/\mu_m = 1.5\times10^4$), the f=0.1 composite ($E_f/\mu_m = 8.0\times10^4$) undergoes significant deformation after tearing (highlighted by dashed white regions), indicating a large energy dissipation zone on the centimeter scale. This result demonstrates that high E_f/μ_m significantly facilitates force transfer over a large distance, allowing extensive energy dissipation throughout this region.

The large, macroscale energy dissipation zone suggested by Figure 3a allows us to investigate the sample size dependence on the tearing behavior, from which we can accurately determine the force transfer length. When the sample width (w) is decreased to a value less than the force transfer length, the tearing resistance starts to decrease with w and the failure behavior of the composites also changes.[20-22] Figure 3b shows the influence of sample size on tearing

energy, T, for the f=0.1 and f=0.3 composites. They are tested from w = 5 mm to increasingly large w until T saturates. Similar to PA hydrogel/glass fabric composites,[22] two characteristic sample widths, w_1 and w_2, are observed (Figure S10, Supporting Information). Fiber fracture starts to occur at w_1 and becomes the main fracture mode at w_2. The tearing energy increases with the sample width w, and saturates at w_2,

$$T = k \cdot w, w < w_2 \quad (2a),$$

$$T = k \cdot w_2, w \geq w_2 \quad (2b).$$

The proportional constant k has a unit of energy dissipation density (J m^{-3}). Equation (2) states that the tearing energy, T, is balanced by the release of stored strain energy in the crack tip zone of length w for samples with width $w < w_2$ or w_2 for samples with width $w \geq w_2$. The saturated T at $w \geq w_2$ gives the intrinsic, size-independent tearing energy, Γ, of the composites. Therefore, the parameters k and w_2 can be associated with the energy dissipation density, W, and the energy dissipation zone size, l_T, as $W = k$ and $l_T = w_2$, respectively, for the relationship shown in Equation (1).

The f=0.1 composite achieves $\Gamma \approx$ 1400 kJ m^{-2} at w_2 = 60 mm. In comparison, the f=0.3 composite attains $\Gamma \approx$ 550 kJ m^{-2} at w_2 = 21 mm. The f=0.1 composite needs a larger w_2 to reach Γ, which indicates a larger force transfer length, in comparison with the f=0.3 composite. These results are consistent with the observation of the dissipation area of samples that undergo tearing (Figure 3a).

To quantitatively understand the parameters k (or W) and w_2 (or l_T), we further investigated the correlation between these two quantities and the mechanical properties of the soft FRPs from different combinations of viscoelastomer matrices and fibers. The chemical structures and mechanical properties of the matrices are shown in Figure 1b, Figure S11, and Table S5 (Supporting Information). The structures and mechanical properties of fabrics are shown in Figure S1, Figure S2, Table S1, and Table S2 (Supporting Information). For simplicity, samples

are denoted as M*i-f*/*xF* for composites made from matrix M*i-f* (*i*=1,2,3) and fiber fabrics *xF* (*xF* =CF, GF, and AF), where CF, GF, and AF stand for carbon fiber, glass fiber, and aramid fiber fabric, respectively. As indicated in Figure S12 (Supporting Information), the tearing energies of all composites measured at different tearing velocities show similar sample width dependence as those in Figure 3b. Summarized w_2 and fiber/matrix property ratios for all composites at different tearing velocities are shown in Table S6 (Supporting Information).

As shown in Figure 3c, the log-log plot of w_2 versus E_f/μ_m for different combinations of fibers and soft matrices at varied tearing velocities shows a linear correlation with a slope of 0.5 for $E_f/\mu_m > 10^4$, following a scaling equation,

$$w_2(mm) = 0.19\,(\frac{E_f}{\mu_m})^{\frac{1}{2}} \quad (3).$$

Positive correlations between w_2 and fracture stress ratio, fracture strain ratio, and fracture energy ratio of fiber to matrix (Figure S13, Supporting Information) also exist, but the strongest correlation is observed with modulus ratio. These results suggest that the modulus ratio is the most relevant quantity to determine the load transfer length in these soft FRPs.

For unidirectional fiber reinforced composites with parallel fibers perfectly bonded to a soft elastic matrix, Hui et al have found theoretically that the force transfer length is proportional to the square root of the fiber/matrix modulus ratio assuming the linear mechanics.[12-14] The scaling relation $w_2 \sim (\frac{E_f}{\mu_m})^{\frac{1}{2}}$ is in good agreement with this theoretical relationship. Furthermore, the pre-factor 0.19 mm in Equation (3) is very close to the theoretical values (0.201~0.208 mm), estimated from the geometry of the composites (Figure S14, Supplementary Appendix, Supporting Information).

In Figure 3c we observe that the two data points with $E_f/\mu_m < 10^4$ show an upward deviation of w_2 from the scaling relation $w_2 \sim (\frac{E_f}{\mu_m})^{\frac{1}{2}}$, which means the force transfer length is greater than predicted from the scaling relation of Equation (3). These data are tested at a high velocity of

500 mm min^{-1}, corresponding to a strain rate of 0.7 s^{-1} in tensile tests. At such high strain rate, the matrices M1-0.3 and M1-0.25 of the composites show high modulus and obvious yielding behavior (Figure S11, Table S5, Supporting Information). Therefore, debonding at the interface occurs easily, and the force transfer is due to topological interlocking between the fabric and the matrix, which needs a wider sample size to reach the critical force for fiber fracture. In fact, SEM observation on the fracture surface of the composite with E_f/μ_m of 6.0×10^2 reveals that no residual matrix remains on the surface of the broken fibers (Figure 3d-i), indicating interfacial debonding during tearing. On the contrary, for the composite with E_f/μ_m of 1.5×10^4, the matrix is still strongly bonded to the fibers even though it undergoes dramatic shear deformation (Figure 3d-ii). These results demonstrate that a soft matrix favors strong bonding to the fabric. With the premise of a strong interface, the force transfer length of FRPs is proportional to the square root of modulus ratio.

Next, we discuss what determines the energy dissipation density W. For tough homogeneous materials, W is related to the work of extension at fracture of the material.[37-40] Since our soft, inhomogeneous composites have very large force transfer lengths (on the cm scale), tensile tests on specimens with conventional cm size should give higher strength and work of extension than the intrinsic values.[14] Therefore, it is not proper to use experimentally obtained tensile data (Figure S15, Table S7, Supporting Information) to determine W. When the composite undergoes tearing, fiber breaking and matrix failure during fiber pullout both contribute to energy dissipation. For the composites studied here, the energy dissipated by the soft, tough matrices can be significant and is on the same order of magnitude as the energy dissipated by fiber breaking (Table S2, Table S5, Supporting Information). Hence, we introduce an effective work of extension, W_{eff}, which is the volume-weighted average of the work of extension of the fiber bundle, W_f, and the matrix, W_m, at fracture.

$$W_{eff} = W_f \cdot V_f + W_m \cdot (1 - V_f) \quad (4),$$

where V_f is the volume fraction of fiber in the composites (50% in this work). W_{eff} is found to be systematically smaller than the work of extension at fracture of the composites, W_c, estimated by testing specimens with a gauge length of 20 mm (Figure S15 and Table S7, Supporting Information). Since the load transfer length is equal to w_2, $l_T = w_2$, we investigated the correlation between the tearing energy, Γ, and the product of $W_{eff} \cdot w_2$. As seen in the plot of Γ versus $W_{eff} \cdot w_2$ for varied soft FRP systems at varied deformation rates (**Figure 4**a), all of the data falls on the straight line of $\Gamma = W_{eff} \cdot w_2$. This result suggests that W_{eff} reflects the energy dissipation density ($W=W_{eff}$). It is also worth noting that the composites with low E_f/μ_m ($< 10^4$) also conform to the correlation although their force transfer length, due to interfacial debonding, does not obey the square root relation with the modulus ratio. This is because even though debonding occurs at the interface, the force transferred by the interlocking structure of the composites also results in fiber breaking, instead of pulling out from matrix, leading to the full energy release of components.

The analysis above demonstrates that maximizing the values of the two important parameters, W and l_T, facilitates the design of extremely tough soft FRPs. This is realized by combining a matrix P(DEEA-*co*-IBA) (M3-0.6) that is adhesive, soft (μ_m = 0.11 MPa), and tough (W_m = 8.3 MJ m^{-3}), with AF fabric that is extremely rigid (E_f = 17 GPa) and strong (σ_f = 1085 MPa, W_f = 56 MJ m^{-3}). W is maximized through the high energy dissipation density of the fiber while l_T is maximized by the extremely high modulus ratio (E_f/μ_m=1.5×10^5). The resulting soft FRP, possessing both high W (W_{eff} = 32 MJ m^{-3}) and l_T (w_2 = 84 mm), achieves a tearing toughness as high as 2500 kJ m^{-2} (Figure 4a), which exceeds the toughest known materials as well as recently developed tough soft FRPs from polyampholyte hydrogels and glass fibers.[20-22]

The force transfer length or the size of the energy dissipation zone of a material is usually expressed by a plot of fracture energy, Γ, versus the work of extension at fracture, W.[41] The slope of the plot reflects the size of the energy dissipation zone, l_T, according to Equation (1).

Here, we show the plot of Γ versus W for various material systems, from soft to rigid in Figure 4b. We used W_{eff} for our soft FRPs. It is obvious that the soft FRPs that contain a viscoelastic matrix, regardless of whether the matrix is polyampholyte (PA) hydrogel or viscoelastomer, show energy dissipation zones approaching 100 mm, which is higher than any common material system.[41-46] In contrast, the traditional soft FRPs from synthetic or natural rubbers can merely achieve energy dissipation zones of about 1 mm. Although their matrices are also soft and fiber/matrix modulus ratio can be quite high, they are not able to reach the theoretical size of the energy dissipation zone due to inefficient load transfer caused by interfacial debonding.[15-17]

The soft FRPs developed in this work also demonstrate an efficient combination of multiple properties. Figure 4c first gathers the tensile modulus of the soft FRPs as a function of density, with other industrial materials for comparison. Together with other type of soft FRPs, the viscoelastomer/fiber composites show lower tensile modulus than ceramics, metallic glasses, CFRP and GFRP, metals and alloys but higher tensile modulus than engineering polymers and elastomers, filling the gap between soft materials and traditional rigid materials. Figure 4d illustrates the fracture energy as a function of density for materials. The viscoelastomer/fiber soft composites show an overwhelming advantage over common industrial structural materials in terms of fracture energy, exceeding those of other materials, either traditional soft FRPs, or rigid materials (CFRP and GFRP, metals and alloys, metallic glasses, and ceramics) by orders of magnitude. Yet the soft FRPs exhibit low density, which is comparable with engineering polymers and elastomers, and even woods. The soft FRPs also show a high tensile strength of 400 to 700 MPa, which is stronger than engineering polymers and elastomers, and rival conventional soft FRPs (Figure 4e). “Specific” mechanical quantities, which are the quantities divided by the density of the materials, are frequently used for the selection of lightweight but strong materials.[47, 48] Figure 4f plots the specific fracture energy of materials as a function of specific strength. The soft FRPs are located in the upper-right corner of the plot, indicating an

excellent combination of high toughness and strength with low weight. The performance of the soft FRPs is superior to all best-in-class industrial materials at present and even exceeds the extremely tough PA gel/fiber composites. These results demonstrate that soft FRPs made from adhesive, tough viscoelastic matrix could overcome the conflict between toughness and weight.

It should be noted that since the viscoelastic properties of a polymer are usually sensitive to the operating temperature and deformation rate, the soft FRPs possessing the best performance should be designed according to the operating temperature and deformation rate. Therefore, developing novel viscoelastomers with broad temperature and dynamic mechanical spectra will greatly expand the practical use of the viscoelastomer-based soft FRPs in industry.

Experimental Section

Experiments details are provided in the Supporting Information.

Supporting Information

Supporting Information is available from the Wiley Online Library or from the author.

Acknowledgements

This research was supported by JSPS KAKENHI Grant Numbers JP17H06144 and JP17H06376. W. C. thanks MEXT, Japan for the scholarship during his PhD study. Institute for Chemical Reaction Design and Discovery (ICReDD) was established by World Premier International Research Initiative (WPI), MEXT, Japan. The authors thank Dr. Yoshinori Katsuyama for setting up testing devices. C.Y. Hui acknowledge support by National Science Foundation (NSF), USA MoMS program under grant number 1903308.

Received: ((will be filled in by the editorial staff))
Revised: ((will be filled in by the editorial staff))
Published online: ((will be filled in by the editorial staff))

References

[1] H. P. Patel, J. L. Turner, J. D. Walter, *Rubber Chem. Technol.* **1976**, *49*, 109510.

[2] X. Li, Y. Wei, Q. Feng, R. K. Luo, *Fibers Polym.* **2017**, *18*, 542.

[3] X. Yang, Z. Zhang, J. Yang, Y. Sun, *SpringerPlus* **2016**, *5*, 1573.

[4] R. V. Silva, D. Spinelli, W. W. Bose Filho, S. Claro Neto, G. O. Chierice, J. R. Tarpani, *Compos. Sci. Technol.* **2006**, *66*, 1328;

[5] S.-H. Lim, A. Dasari, Z.-Z. Yu, Y.-W. Mai, S. Liu, M. S. Yong, *Compos. Sci. Technol.* **2007**, *67*, 2914.

[6] J. W. Hutchinson, Z. Suo, *Adv. Appl. Mech.* **1991**, *29*, 63.

[7] R. Long, C.-Y. Hui, *Soft Matter* **2016**, *12*, 8069.

[8] C. Creton, M. Ciccotti, *Rep. Prog. Phys.***2016**, *79*, 046601.

[9] Z. Wang, C. Xiang, X. Yao, P. Le Floch, J. Mendez, Z. Suo, *Proc. Natl. Acad. Sci. USA* **2019**, *116*, 5967.

[10] A. Thomas, *J. Polym. Sci.* **1955**, *18*, 177.

[11] K. Volokh, P. Trapper, *J. Mech. Phys. Solids* **2008**, *56*, 2459.

[12] J. M. Hedgepeth, *NASA TN D-882* **1961**.

[13] H. Cox, *Br. J. Appl. Phys.* **1952**, *3*, 72.

[14] C.-Y. Hui, Z. Liu, S. L. Phoenix, *Extreme Mech. Lett.* **2019**, *33*, 100573.

[15] M. L. Mehan, L. S. Schadler, *Compos. Sci. Technol.* **2000**, *60*, 1013.

[16] Q. Meng, M. Chang, *Int. J. Solids Struct.* **2019**.

[17] R. Pan, D. Watt, *Polym. Compos.* **1996**, 17, 486.

[18] W. R. K. Illeperuma, J.-Y. Sun, Z. Suo, J. J. Vlassak, *Extreme Mech. Lett.* **2014**, *1*, 90.

[19] J. Moraleda, J. Segurado, J. Llorca, *Int. J. Solids and Struct.* **2009**, *46*, 4287.

[20] D. R. King, T. L. Sun, Y. Huang, T. Kurokawa, T. Nonoyama, A. J. Crosby, J. P. Gong, *Mater. Horiz.* **2015**, *2*, 584.

[21] Y. Huang, D. R. King, T. L. Sun, T. Nonoyama, T. Kurokawa, T. Nakajima, J. P. Gong, *Adv. Funct. Mater.* **2017**, *27*, 1605350.

[22] Y. Huang, D. R. King, W. Cui, T. L. Sun, H. Guo, T. Kurokawa, H. R. Brown, C.-Y. Hui, J. P. Gong, *J. Mater. Chem. A* **2019**, *7*, 13431.

[23] T. L. Sun, T. Kurokawa, S. Kuroda, A. B. Ihsan, T. Akasaki, K. Sato, M. A. Haque, T. Nakajima, J. P. Gong, *Nat. Mater.* **2013**, *12*, 932.

[24] C. K. Roy, H. L. Guo, T. L. Sun, A. B. Ihsan, T. Kurokawa, M. Takahata, T. Nonoyama, T. Nakajima, J. P. Gong, *Adv. Mater.* **2015**, *27*, 7344.

[25] L. Chen, T. L. Sun, K. Cui, D. R. King, T. Kurokawa, Y. SARUWATARI, J. P. Gong, *J. Mater. Chem. A* **2019**, *7*, 17334.

[26] A. N. Gent, G. S. Fielding-Russell, D. I. Livingston, D. W. Nicholson, *J. Mater. Sci.* **1981**, *16*, 949.

[27] A. N. Gent, G. L. Liu, *J. Mater. Sci.* **1991**, *26*, 2467.

[28] E. Triki, P. Dolez, T. Vu-Khanh, *Compos. Part B-Eng.* **2011**, *42*, 1851.

[29] E. Triki, T. Vu-Khanh, P. Nguyen-Tri, H. Boukehili, *Theor. Appl. Fract. Mec.* **2012**, *61*, 33.

[30] A. M. Hubbard, W. Cui, Y. Huang, R. Takahashi, M. D. Dickey, J. Genzer, D. R. King, J. P. Gong, *Matter* **2019**, *1*, 674.

[31] D. C. Hofmann, J.-Y. Suh, A. Wiest, G. Duan, M.-L. Lind, M. D. Demetriou, W. L. Johnson, *Nature* **2008**, *451*, 1085.

[32] L.-B. Mao, H.-L. Gao, H.-B. Yao, L. Liu, H. Cölfen, G. Liu, S.-M. Chen, S.-K. Li, Y.-X. Yan, Y.-Y. Liu, *Science* **2016**, *354*, 107.

[33] L. Xu, X. Zhao, C. Xu, N. A. Kotov, *Adv. Mater.* **2018**, *30*, 1703343.

[34] M. D. Demetriou, M. E. Launey, G. Garrett, J. P. Schramm, D. C. Hofmann, W. L. Johnson, R. O. Ritchie, *Nat. Mater.* **2011**, *10*, 123.

[35] B. L. Smith, T. E. Schäffer, M. Viani, J. B. Thompson, N. A. Frederick, J. Kindt, A. Belcher, G. D. Stucky, D. E. Morse, P. K. Hansma, *Nature* **1999**, *399*, 761.

[36] E. Munch, M. E. Launey, D. H. Alsem, E. Saiz, A. P. Tomsia, R. O. Ritchie, *Science* **2008**, *322*, 1516.

[37] J.-Y. Sun, X. Zhao, W. R. Illeperuma, O. Chaudhuri, K. H. Oh, D. J. Mooney, J. J. Vlassak, Z. Suo, *Nature* **2012**, *489*, 133.

[38] C. Chen, Z. Wang, Z. Suo, *Extreme Mech. Lett.* **2017**, *10*, 50.

[39] C. Yang, T. Yin, Z. Suo, *J. Mech. Phys. Solids* **2019**, *131*, 43.

[40] J. Liu, C. Yang, T. Yin, Z. Wang, S. Qu, Z. Suo, *J. Mech. Phys. Solids* **2019**, *133*, 103737.

[41] M. F. Ashby, *MRS Bull.* **2005**, *30*, 995.

[42] Á. Kmetty, T. Bárány, J. Karger-Kocsis, *Prog. Polym. Sci.* **2010**, *35*, 1288.

[43] R. O. Ritchie, *Nat. Mater.* **2011**, *10*, 817.

[44] J. Schroers, W. L. Johnson, *Phys. Rev. Lett.* **2004**, *93*, 255506.

[45] B. Gludovatz, A. Hohenwarter, D. Catoor, E. H. Chang, E. P. George, R. O. Ritchie, *Science* **2014**, *345*, 1153.

[46] W. Clegg, K. Kendall, N. M. Alford, T. Button, J. Birchall, *Nature* **1990**, *347*, 455.

[47] X. Zhang, A. Vyatskikh, H. Gao, J. R. Greer, X. Li, *Proc. Natl. Acad. Sci. USA* **2019**, *116*, 6665.

[48] X. Zhang, L. Zhong, A. Mateos, A. Kudo, A. Vyatskikh, H. Gao, J. R. Greer, X. Li, *Nat. Nanotechnol.* **2019**, *14*, 762.

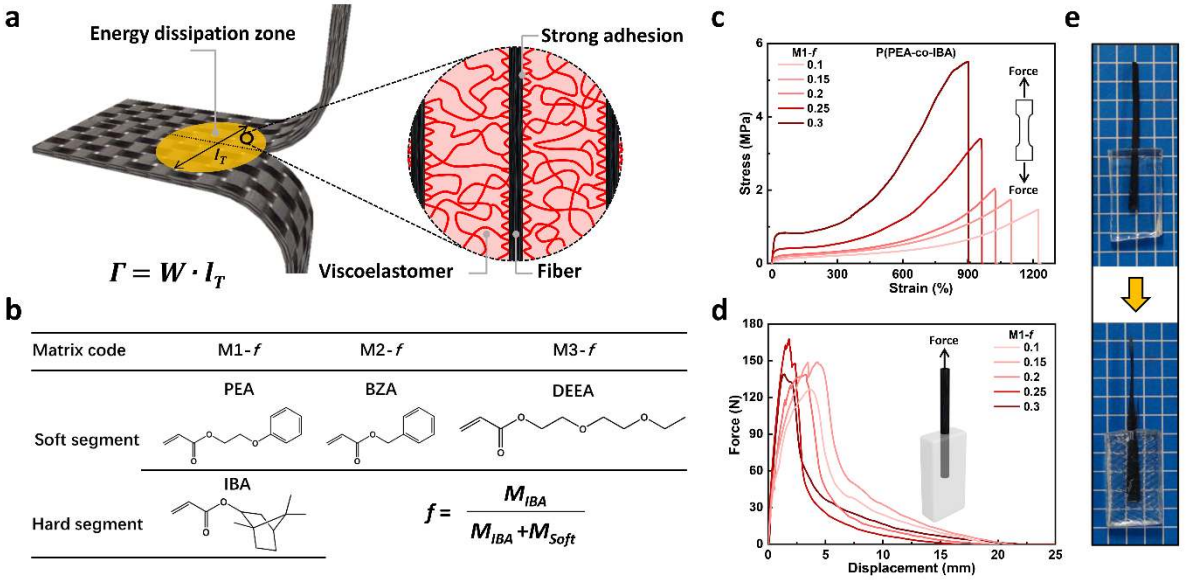

Figure 1. Design strategy of extraordinarily tough fiber-reinforced polymers (FRPs) and the properties of viscoelastomer matrices. a) The strategy employed involves combining strong and rigid woven fabrics with viscoelastomer matrices that are adhesive, soft, and tough. Such a combination gives high energy dissipation density, W and large energy dissipation zone, l_T (on the cm scale) due to the high fiber/matrix modulus ratio (10^4~10^5), guaranteed by the strong fiber/matrix interface. b) Monomer structures that make up the viscoelastomer matrices. Each matrix is produced from copolymerizing a soft segment (ethylene glycol phenyl ether acrylate (PEA), benzyl acrylate (BZA), or di(ethylene glycol) ethyl ether acrylate (DEEA)) with a hard segment (isobornyl acrylate (IBA)). The molar fraction of the hard segment is defined as *f*. c) Tunable tensile properties of the copolymer P(PEA-*co*-IBA) with various *f* (coded M1-*f*). The displacement velocity and strain rate of the tensile tests were 50 mm min^{-1} and 0.07 s^{-1}, respectively. d) Adhesion tests to determine the interfacial bonding strength between single carbon fiber bundles and matrices, M1-*f*. A carbon fiber bundle was embedded in the transparent matrix with an embedded surface area of 3.8 mm (cross-sectional perimeter) × 15 mm (length). The testing velocity was 50 mm min^{-1}. e) Images showing the samples before and after the adhesion test. The background grid size is 5 mm. In (d) and (e), the fiber bundle fractures without being pulled out from the matrix, indicating the high strength of the interface as well as the matrices.

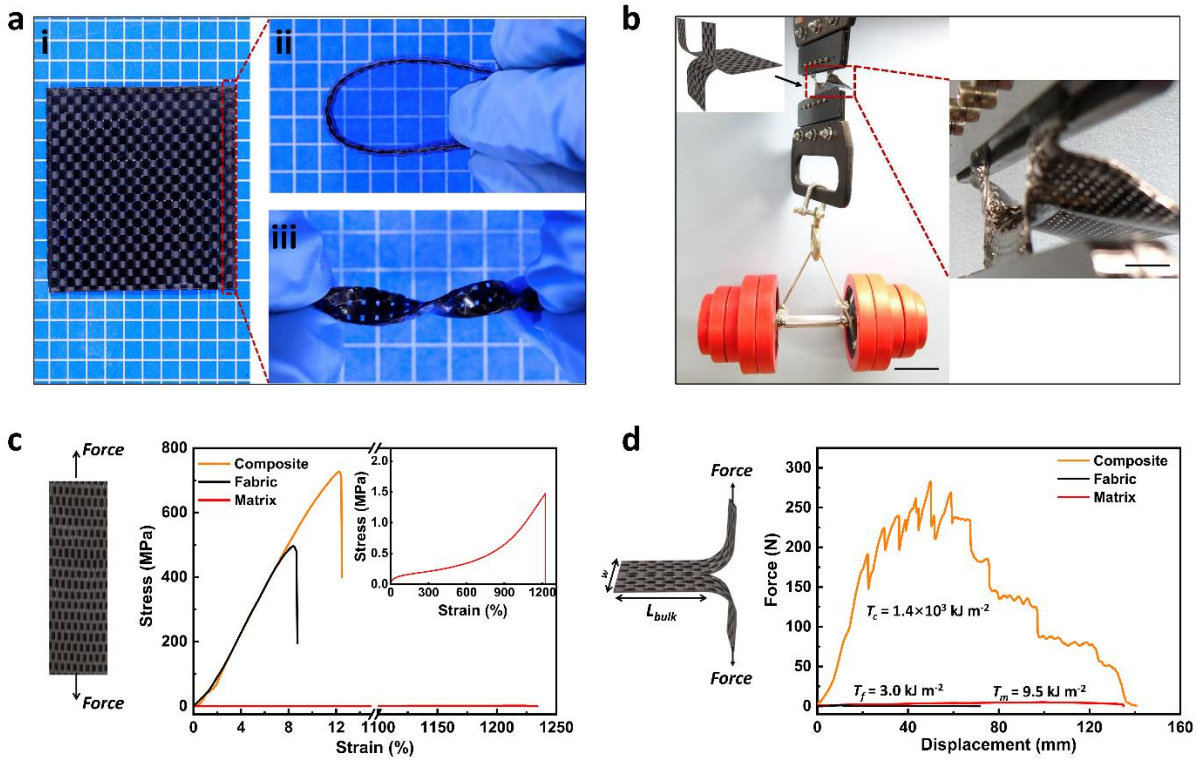

Figure 2. Demonstration of the superior mechanical properties of soft FRPs. a) The appearance and anisotropy of the composite made from CF and matrix M1-0.1. (i) The fabric is visible because the matrix is optically transparent. (ii) and (iii) A strip of the composite is cut to clearly show its flexibility under bending or twisting. The background grid size is 5 mm. b) A demonstration of the extraordinary crack resistance of the composite. A composite specimen with two cracks can sustain 35 kg of weight without crack propagation. The scale bars represent 10 cm. c) Tensile tests on the composite, neat fabric, and neat matrix, with 10 mm sample width, measured at strain velocity and strain rate of 50 mm min^{-1} and 0.07 s^{-1}, respectively. The composite shows improved strength and work of extension in comparison to the neat fabric. d) Trouser tearing tests on the composite, neat fabric and neat matrix. Samples are prepared with a width (w) of 50 mm, and a length of 80 mm. A pre-notch of 30 mm is made in the middle of the sample to make the projected length of tear (L_{bulk}) equal to width. Force-displacement curves show that the composite has much higher tearing strength and energy than the neat fabric and matrix. The tearing velocity was 50 mm min^{-1}.

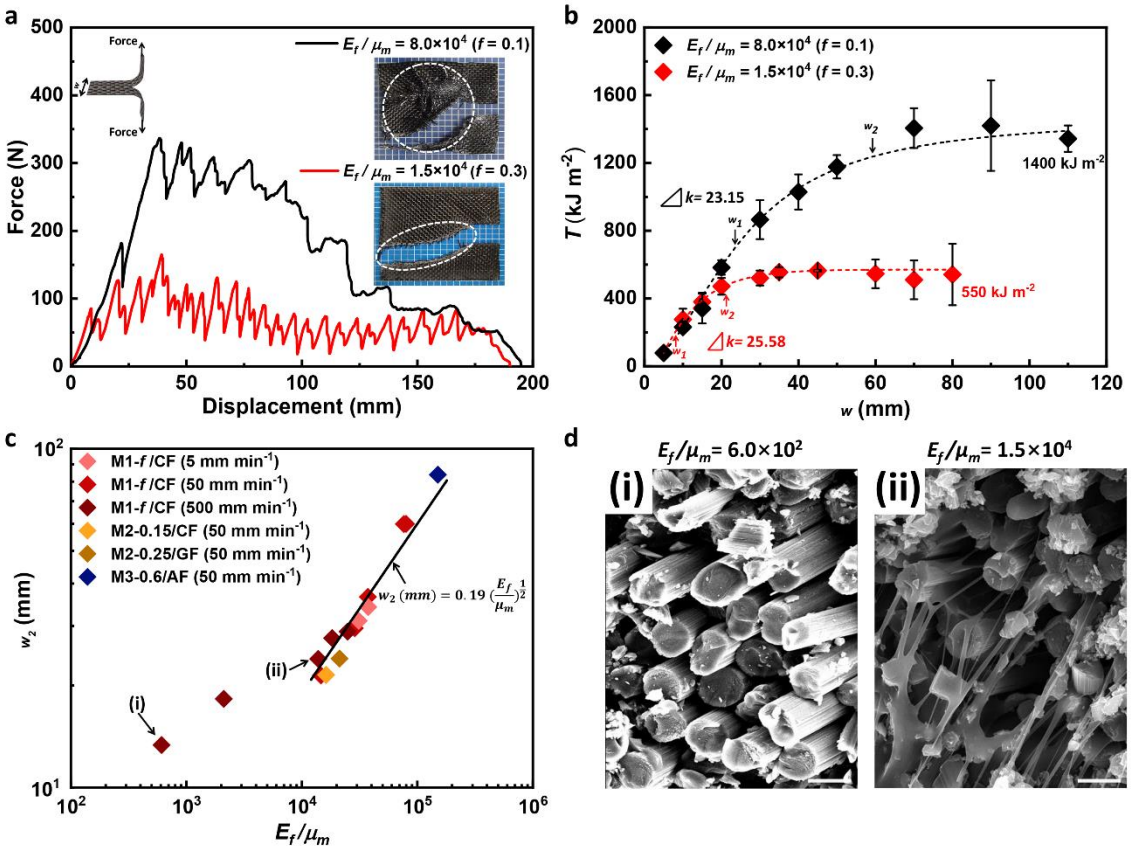

Figure 3. Influence of fiber/matrix modulus ratio on the size of the energy dissipation zone of soft FRPs. a) Representative force-displacement curves of trouser tearing tests on composites from CF and M1-*f* with different modulus ratios, E_f/μ_m. Comparing composites made from M1-0.3, composites made from M1-0.1 with high modulus ratio show a higher tearing force as well as a larger deformation zone indicated by the inset images, suggesting a larger force transfer length. The inset background grid size is 5 mm. Tearing velocity was 50 mm min^{-1}. b) Composite toughness as measured by tearing energy, T as a function of sample size, w. T increases with w and reaches the saturation toughness $T = \Gamma$ at a critical size that is related to the size of energy dissipation zone of the composite, $w_2 = l_T$. The composite with high modulus ratio reaches a higher saturation toughness at a larger w. Tearing velocity was 50 mm min^{-1}. c) Correlation between the size of the energy dissipation zone, determined by w_2, and the modulus ratio for composites from various combinations of fabrics and matrices that are measured at different velocities. For composites with modulus ratio larger than 10^4, w_2 is proportional to the square root of the modulus ratio, w_2 (mm) = 0.19 $(E_f/\mu_m)^{1/2}$. CF, GF, and AF stand for carbon, glass, and aramid fiber fabrics, respectively. d) SEM images of fractured surfaces for composites shown in (c) by (i) and (ii). For composites made from the relatively rigid matrix (μ_m = 35.1 MPa) and having low modulus ratio, debonding occurs when fibers are fractured and pulled out (i). On the contrary, for composites from the soft matrix (μ_m = 1.5 MPa) and having high modulus ratio, the matrix is still strongly bonded when fibers are fractured and pulled out (ii). Scale bars represent 10 μm.

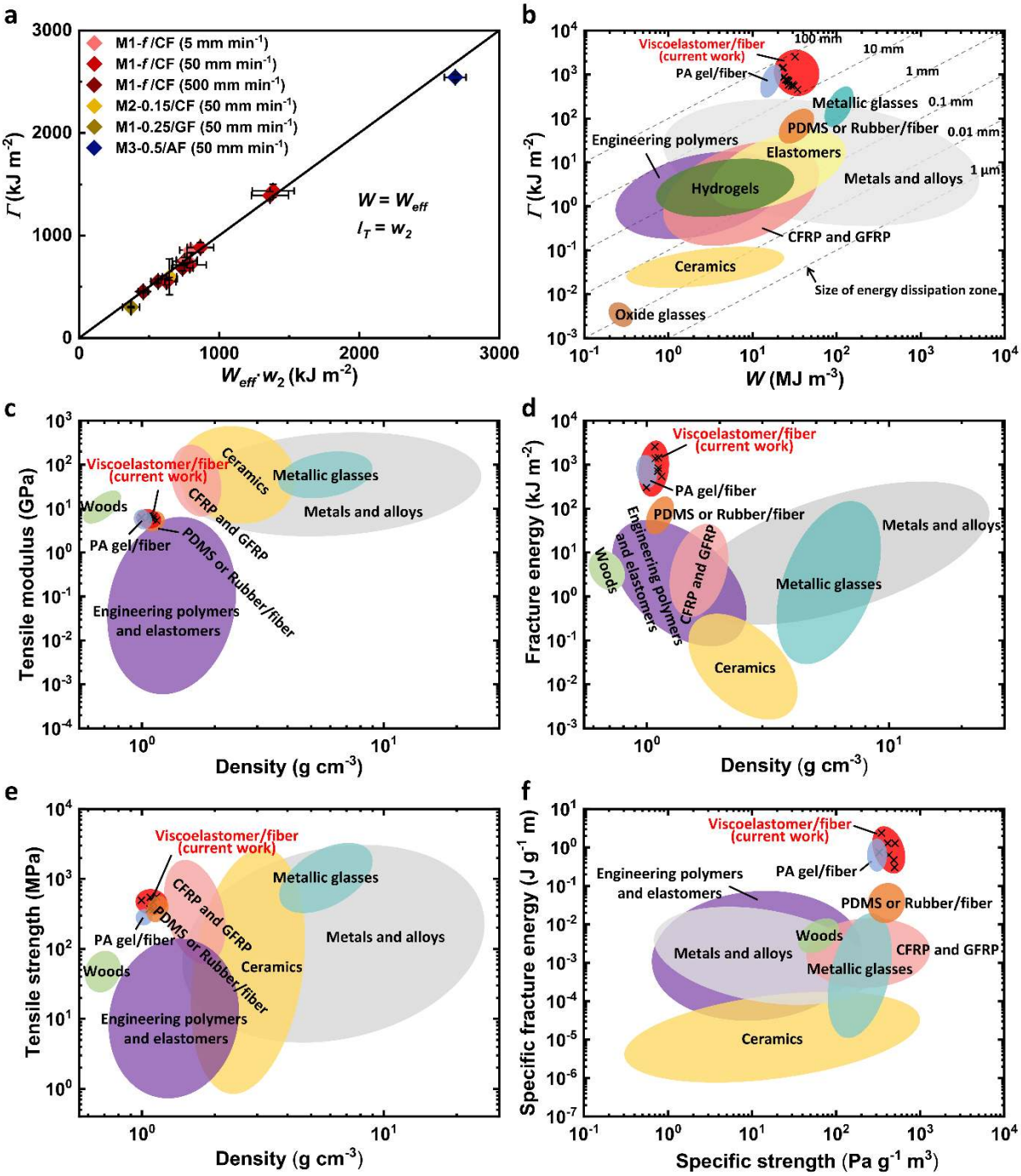

Figure 4. Comparison of the size of the energy dissipation zone and mechanical properties for various tough materials. a) The experimentally determined saturation toughness, Γ of soft FRPs versus $W_{eff} \cdot w_2$, where W_{eff} is the volume weighed average of the work of extension of the fiber bundle and the matrix at fracture, and w_2 is the experimentally determined size of the energy dissipation zone (force transfer length). The validity of $\Gamma = W_{eff} \cdot w_2$ indicates the energy dissipation density W and the size of energy dissipation zone l_T shown in Equation (1) is related to W_{eff} and w_2, respectively. b) Γ of various materials versus energy dissipation density, W. The slopes shown by the dotted lines reflect the size of the energy dissipation zone of different materials. c) Tensile modulus (E) versus density (ρ). d) Fracture energy (Γ) versus density. e) Tensile strength (σ) versus density. f) Specific fracture energy (Γ/ρ) versus specific strength (σ/ρ). Fracture energies of various materials were determined by trouser tearing tests (for soft FRPs from viscoelastomers, PA gels and PDMS, rubbers),[20-22] essential work of fracture (EWF) tests (for engineering polymers and elastomers),[25, 42] double cantilever beam or crack opening three point bend tests (for CFRP and GFRP,[41] metallic glasses,[31, 43, 44] metals and alloys,[41, 45] ceramics,[36, 46] and woods[41]), respectively. Summarized mechanical properties of materials are shown in Table S8 (Supporting Information).

ToC

Novel soft FRPs are developed by using viscoelastic polymers that are adhesive, soft, and tough as matrices. The unique combination of these properties in the matrices ensures a strong component interface, which consequently maximizes the energy dissipation density and gives rise to a large force transfer length enabled by the extremely high fiber/matrix modulus ratio. As a result, the soft FRPs can achieve toughness of up to 2500 kJ m^{-2}, exceeding any existing best-in-class materials.

Keyword: soft fiber-reinforced polymers, extraordinary crack resistance, modulus ratio, force transfer length, energy dissipation density

W. Cui, D.R. King, Y. Huang, L. Chen, T.L. Sun, Y. Guo, Y. Saruwatari, C-Y. Hui, T. Kurokawa, J.P. Gong*

Fiber-reinforced Viscoelastomers Show Extraordinary Crack Resistance that Exceeds Metals

ToC entry figure

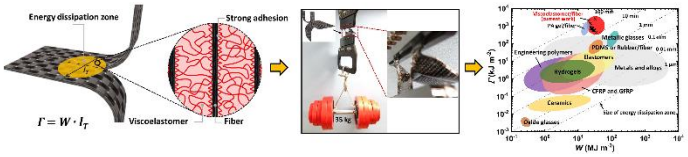

Supporting Information

Fiber-reinforced Viscoelastomers Show Extraordinary Crack Resistance that Exceeds Metals

*Wei Cui, Daniel R. King, Yiwan Huang, Liang Chen, Tao Lin Sun, Yunzhou Guo, Yoshiyuki Saruwatari, Chung-Yuen Hui, Takayuki Kurokawa, and Jian Ping Gong**

Table of contents

Materials and methods (page 2)

Appendix (page 6)

Figure S1-S15 (page 7-21)

Table S1-S8 (page 22-29)

References (page 30)

1. Materials and methods

Materials:

Plain weave carbon fiber fabric (CF), glass fiber fabric (GF), and aramid fiber fabric (AF) were purchased from Marukatsu Co., Ltd., Japan. All fabrics were used as received. The textures of the fabrics are shown in **Figure S1**. Mechanical properties of fabrics and single fiber bundles are shown in **Figure S2** and are summarized in **Table S2**. Acrylate monomers, ethylene glycol phenyl ether acrylate (PEA), benzyl acrylate (BZA), di(ethylene glycol) ethyl ether acrylate (DEEA), and isobornyl acrylate (IBA) were provided by Osaka Organic Chemical Industry Ltd, Japan. Ultraviolet initiator benzophenone (BP) was purchased from KANTO Chemical Co., Inc and used without further purification. Mechanical properties of viscoelastomers prepared from these monomers are shown in **Figure S11** and summarized in **Table S5**.

Methods:

Preparation of fiber-reinforced viscoelastomers. Samples were prepared by placing two 0.5 mm spacers on both sides of the fabric, which was inserted between two hydrophobic films supported by glass plates to form a reaction mold. Subsequently two monomers, one of the following of ethylene glycol phenyl ether acrylate (PEA), benzyl acrylate (BZA), or di(ethylene glycol) ethyl ether acrylate (DEEA), along with isobornyl acrylate (IBA), containing initiator (0.1 mol% of the total monomer molar concentration) was injected into the mold. The random copolymerization was allowed to proceed under an argon atmosphere via

ultraviolet irradiation (UVP lamp Toshiba-FL15BLB, wavelength 365 nm, light intensity 4 mW cm^{-2}) for 10 h. Neat elastomers were also prepared as controls. We confirmed that 1.5 h is enough to form a viscoelastomer that shows its intrinsic mechanical property (**Figure S3**). A typical preparation procedure is shown in Supplementary **Figure S6a**.

Differential Scanning Calorimetry. The glass transition temperature (T_g) of the viscoelastomers were measured by DSC (TA instrument, DSC 2500). The sample of 5-10 mg was placed in a non-hermitic pan, and an empty pan was used as a reference. The DSC experiment was performed in a heat-cool cycle (isothermal -50 °C, 5 min; -50 to 70 °C, 10 °C min^{-1}; isothermal 70 °C, 5 min; 70 to -50 °C, 10 °C min^{-1}; isothermal -50 °C, 5 min; isothermal 70 °C; jump to 20 °C), wherein the thermal transitions for the heating cycle were recorded. The glass transition temperature (T_g) was determined by the inflection point of the heat capacity with temperature sweep.

Uniaxial tensile tests. For composites and fabrics, rectangular-shaped samples (10 mm wide and 80 mm length) were prepared with the fibers aligned parallel or perpendicular to the length direction. Tests were performed on a commercial tensile tester (Autograph AG-X, Shimadzu Co., Japan) equipped with a 20 kN load cell in the open atmosphere at room temperature. The initial length of the sample between grips was 20 mm. Since the fracture for the composite samples occurs at a small strain, and the load supported by the soft matrix at this strain is extremely low, the fracture strength of the composites is calculated from the

maximum load divided by the cross-sectional area of neat fabric before loading (the width, *w*, multiplied by the fabric thickness, *t*) for both the neat fabric and the composite. The work of extension is defined as the area below the obtained stress-strain curve. The crosshead velocity was 50 mm min^{-1}, unless otherwise stated. For viscoelastomers, the tensile tests were carried out by using the same commercial tensile tester equipped with a 100 N load cell at 50 mm min^{-1} crosshead velocity in air. Before the tests, the viscoelastomers were cut into a dumbbell shape standardized as JIS-K6251-7 (2 mm in inner width, 12 mm in gauge length) with a cutting machine (Dumb Bell Co., Ltd.).

Trouser tearing tests. The tearing fracture energy of the samples was evaluated by trouser tearing tests. The tensile tester (Autograph AG-X, Shimadzu Co., Japan) equipped with a 20 kN load cell was employed to perform the tearing tests. A sample with a prescribed width *w* and length *w* + 30 mm was prepared. An initial notch of 30 mm was made in the middle of the sample along the length direction with a laser cutter. For neat elastomer samples, to prevent elongation of the legs during tests, stiff and thin tape was glued on both sides of the samples before testing. During testing, one leg of the sample was clamped to the base, and the other was clamped to the crosshead, which was displaced at a velocity of 50 mm min^{-1} at room temperature in the open atmosphere. After testing, the tearing force-displacement curves were obtained to calculate the tearing energy of samples by the following equation:[1-3]

$$T = \frac{\int_0^L F\, dL}{t \cdot L_{bulk}} \quad \text{(S1)},$$

where F is the tearing force, t is the sample thickness, L is the displacement, and L_{bulk} is the projected crack length.

Three-point bend tests. The flexibility of the composites was examined by three-point bend tests using a tensile tester (Tensilon RTC-1150A, Orientec Co., Japan) equipped with a 100 N load cell in the open atmosphere. The sample width was 10 mm and the length between bottom points was 20 mm. The testing velocity was 30 mm min^{-1}.

Scanning electron microscopy. Microscale observation was carried out by scanning electron microscopy (SEM) (JEOL JSM-6010LA, Tokyo, Japan). Samples were gold-coated in an ion-sputtering machine (E-1010, Hitachi, Tokyo, Japan) before observation. The acceleration voltage varied from 15 to 20 kV.

2. Appendix

Comparison with the theoretical load transfer length for a model composite:

The theoretical load transfer length l_T for a model composite consisting of parallel fibers embedded in a soft matrix is derived in the literature:[4-6]

$$l_T = \sqrt{\frac{E_f A_f d}{\mu_m h}} \quad \text{(S2)},$$

where E_f and μ_m are the tensile modulus of the fiber and the shear modulus of the matrix, respectively, d is the effective distance between adjacent fibers, h is the width of the fiber, and A_f is the cross-sectional area of the fiber. **Equation S2** can also be expressed in terms of the product of the geometric pre-factor $\alpha = \sqrt{\frac{A_f d}{h}}$ and the modulus ratio, as

$$l_T = \alpha \sqrt{\frac{E_f}{\mu_m}} \quad \text{(S3)}.$$

Assuming that this model is applicable to our composites, using the geometry parameters of fabrics shown in **Table S1**, the geometric pre-factors for CF, GF, and AF are estimated as α_{CF} =0.208 mm, α_{GF} =0.206 mm, α_{AF} =0.201 mm, respectively. These values are very close to the pre-factor 0.19 mm observed for $w_2(mm) = 0.19\sqrt{\frac{E_f}{\mu_m}}$ (**Figure 3c** in manuscript). The geometry parameters of fabrics are determined from the cross section of corresponding composites shown in **Figure S14**.

3. Supplementary results

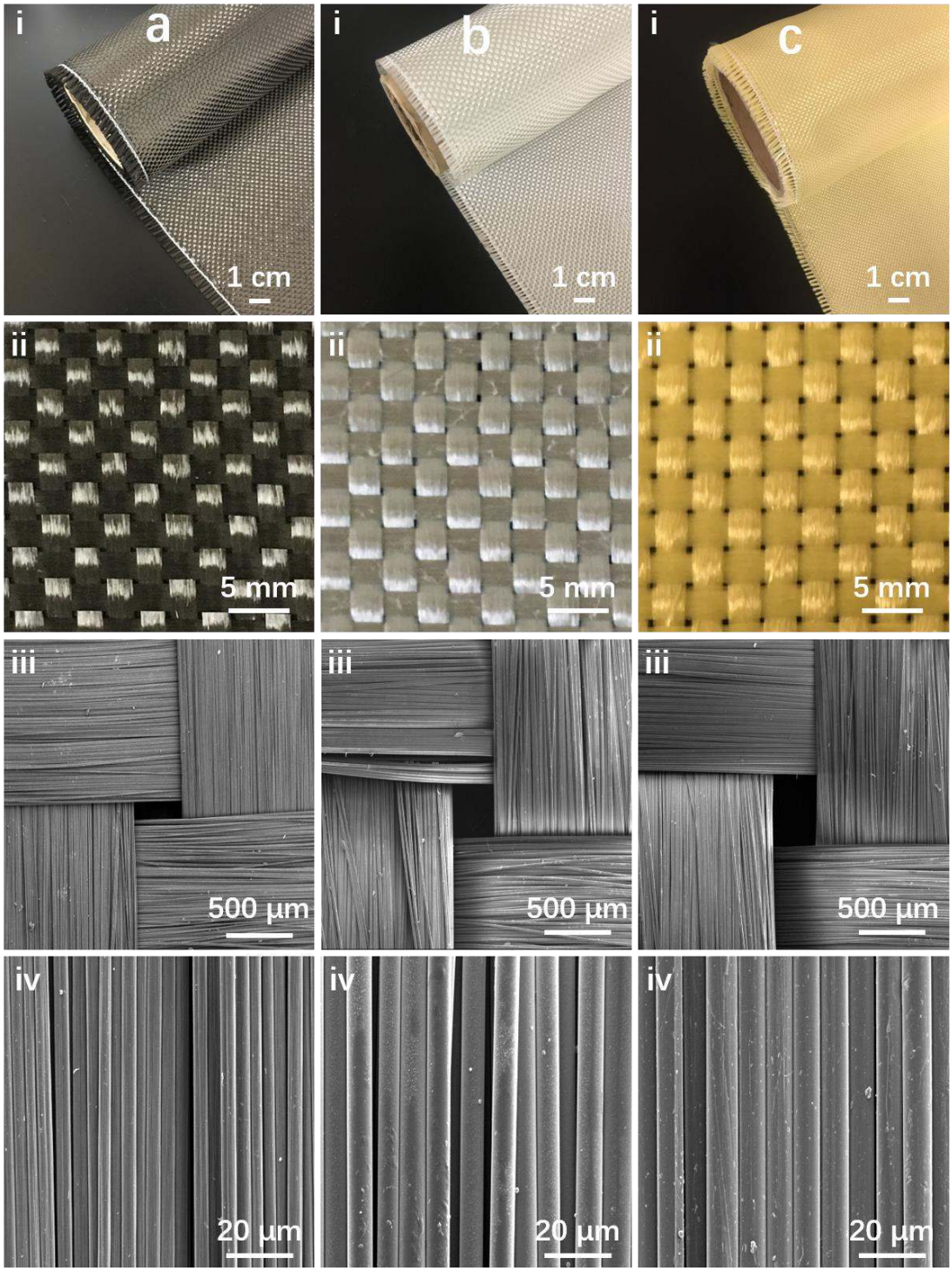

Figure S1. Macro- and micrographs of plain weave (a) carbon fiber (CF), (b) glass fiber (GF), and (c) aramid fiber (AF) fabrics used in this work. All fabrics are in a plane weave pattern of fiber bundles that contains thousands of individual thin fibers. (i) The macrographs of all fabrics. (ii) The plain weave structures. (iii) SEM micrographs of woven fiber bundles. (iv) Individual fibers. The structure parameters of all fabrics are summarized in **Table S1**.

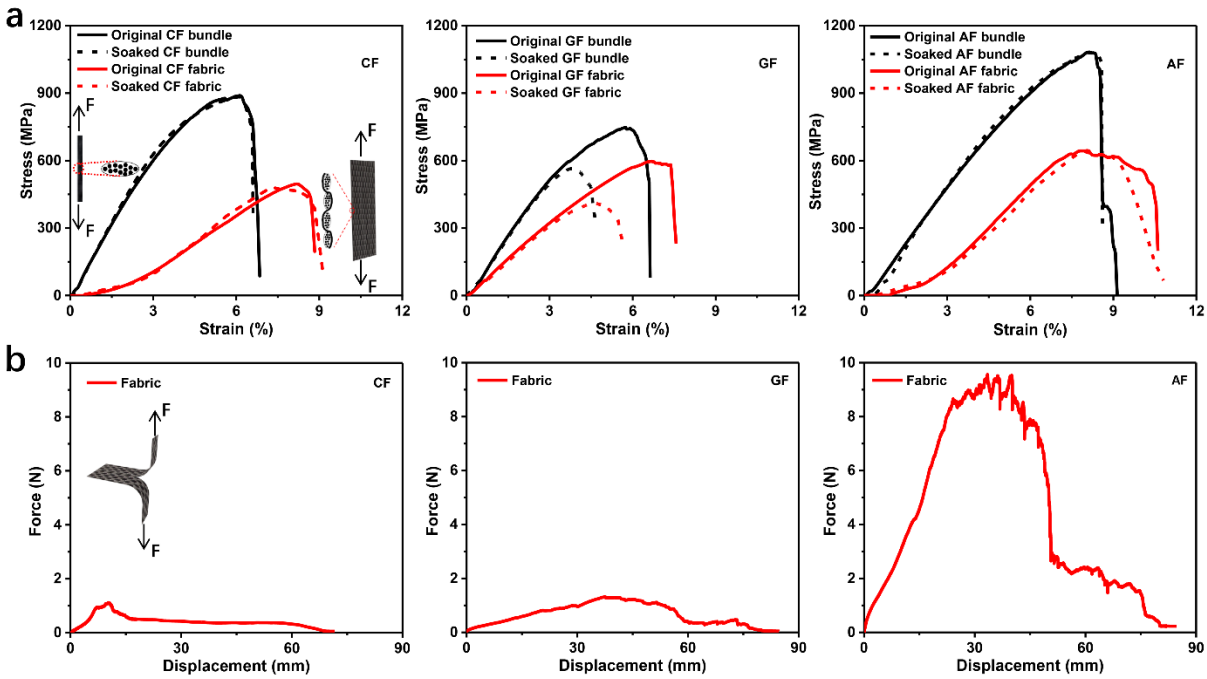

Figure S2. Mechanical properties of woven fabrics and individual fiber bundles used in this work. (a) Tensile stress-strain curves for both fabrics and individual fiber bundles of carbon fiber (CF), glass fiber (GF), and aramid fiber (AF) fabrics. The measurement of the fabrics was performed along the axis of meshes. The tensile performance of a single fiber bundle is different from a fabric. For the fabric that is in a weave pattern, the bundles are in a curved geometry to form meshes. The mesh geometry influences the area to calculate stress and corresponding tensile modulus while the curved geometry influences the strain. Therefore, the fabric shows a lower tensile modulus, fracture stress but higher fracture strain. In particular, tensile properties of GF fabric and individual bundle are influenced by the monomer solution while CF and AF are not. Both GF fabric and bundle show decreased tensile stress and strain after soaking in the monomer solution for 10 h. This can be due to the corrosion of coating on GF during soaking, which generates more defects on GF. Therefore, data for GF after soaking is employed in the whole text. (b) Trousers tearing force-displacement curves for CF, GF, and AF fabrics. Tensile and tearing velocity were both 50 mm min^{-1}. Strain rate for tensile tests was 0.07 s^{-1}. The mechanical properties of all fabrics and fiber bundles are summarized in **Table S2**.

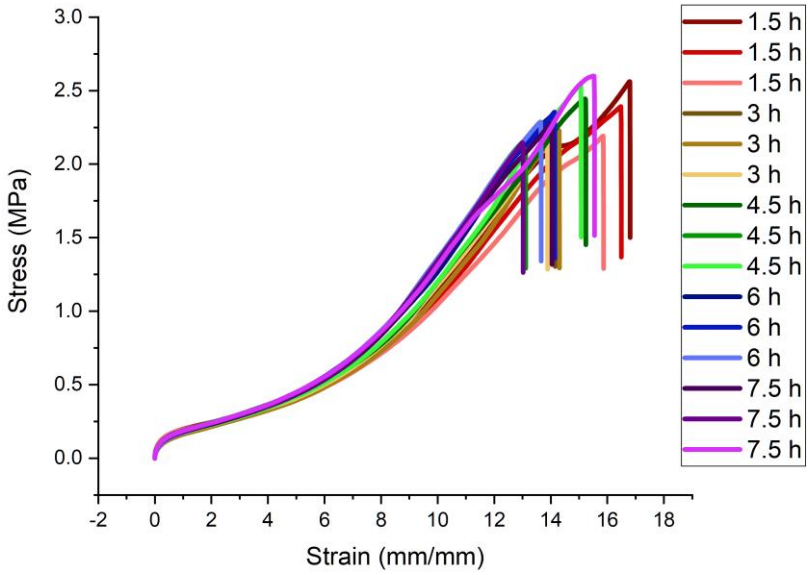

Figure S3. Influence of polymerization time on the mechanical properties of viscoelastomer PPEA. The results show that 1.5 h is enough to generate the viscoelastomer that shows its intrinsic mechanical properties.

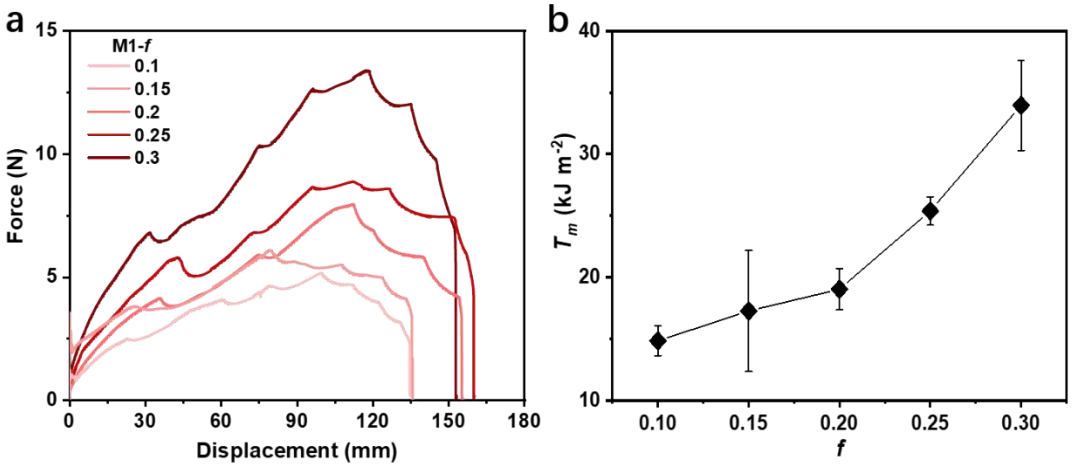

Figure S4. Tailoring mechanical properties of P(PEA-co-IBA) viscoelastomers by tuning molar fraction of IBA (*f*). (a) Tearing properties of P(PEA-co-IBA) with varied *f*. (b) The tearing fracture energy increases with increasing *f*. The velocity of tearing tests was 50 mm min^{-1}. The mechanical properties of all matrices used in this work are summarized in **Table S5**. As indicated in **Figure S4b**, the tearing fracture energy T_m, measured by trousers tearing test at a velocity of 50 mm min^{-1}, can be tuned from 15 to 34 kJ m^{-2}. The tensile modulus (E_m) and the tensile work of extension (W_m) of P(PEA-co-IBA), measured at a strain rate of 0.07 s^{-1}, vary from 0.8 to 4.4 MPa and from 6 to 19 MJ m^{-3}, respectively (**Figure 1c** in manuscript). Therefore, the soft viscoelastomers P(PEA-co-IBA) are highly energy-dissipative, having a work of extension roughly on the order of the rigid CF fiber. In addition, the fiber/matrix modulus ratio, E_f/μ_m, can be as high as $8.0\times10^4 \sim 1.5\times10^4$ when the molar fraction of IBA, *f*, is varied from 0.1 to 0.3. Accordingly, the combination of the CF and the viscoelastomers is expected to give high energy dissipation density and large force transfer length.

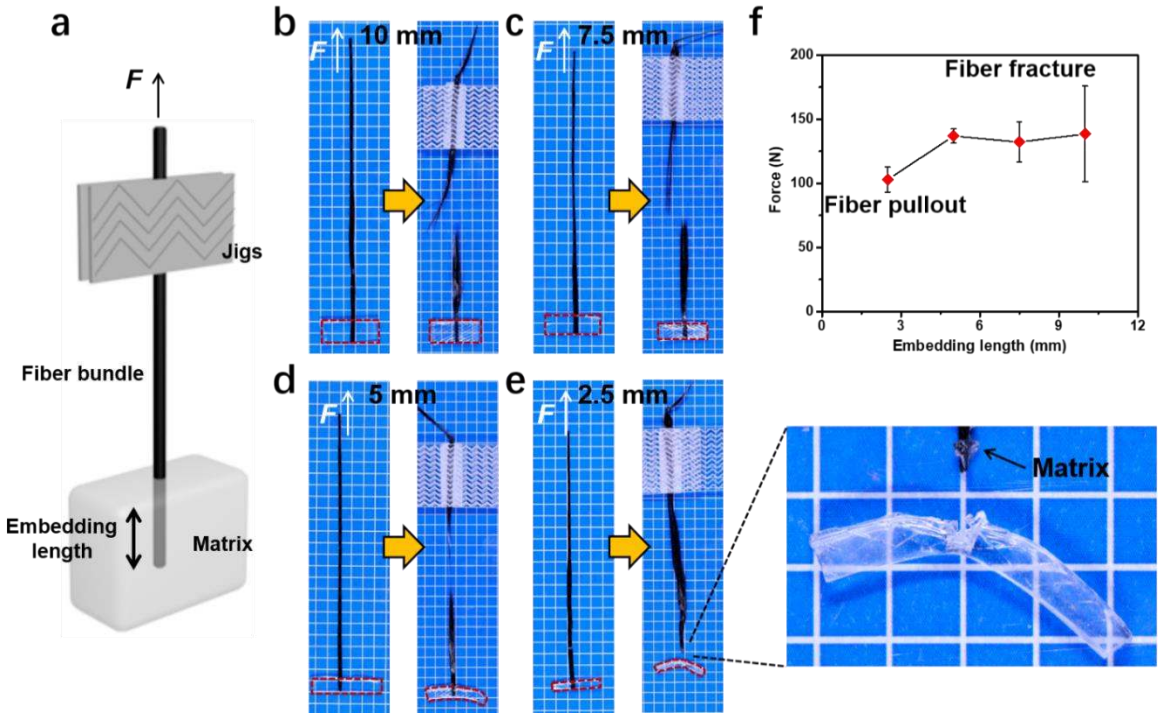

Figure S5. Adhesion test to determine the interfacial strength between M1-0.2 matrix and carbon fiber bundle by varying the embedding length of the fiber.[7, 8] (a) Illustration of the experimental setup for the adhesion test. The embedding length is decreased from 10 mm to 2.5 mm, and the pulling velocity was 50 mm min^{-1}. (b) to (e): A transition of fiber rupture to fiber pullout is found, from which the critical interfacial strength between fiber/matrix components can be determined. The transparent matrix is highlighted by the red dashed rectangle. It is noted that fiber pullout is induced by matrix fracture instead of interface failure when the embedding length is 2.5 mm, as illustrated in the enlarged photo. (f) The adhesion force undergoes a rise when the embedding length increases, corresponding to the transition of failure behavior of the adhesion test. According to the pullout result at embedding length of 2.5 mm, the shear bonding strength (τ_s) of the interface is 11.9 MPa, which is estimated by balancing the external force (F = 113 N) with the adhesion force provided by the shear bonding strength, as $F = \tau_s \cdot A$, where A is the embedded surface area of the fiber bundle. The interfacial strength is well above the matrix strength (2.2 MPa), indicating a strong interface between soft matrices and rigid fibers. The background grid size is 5 mm.

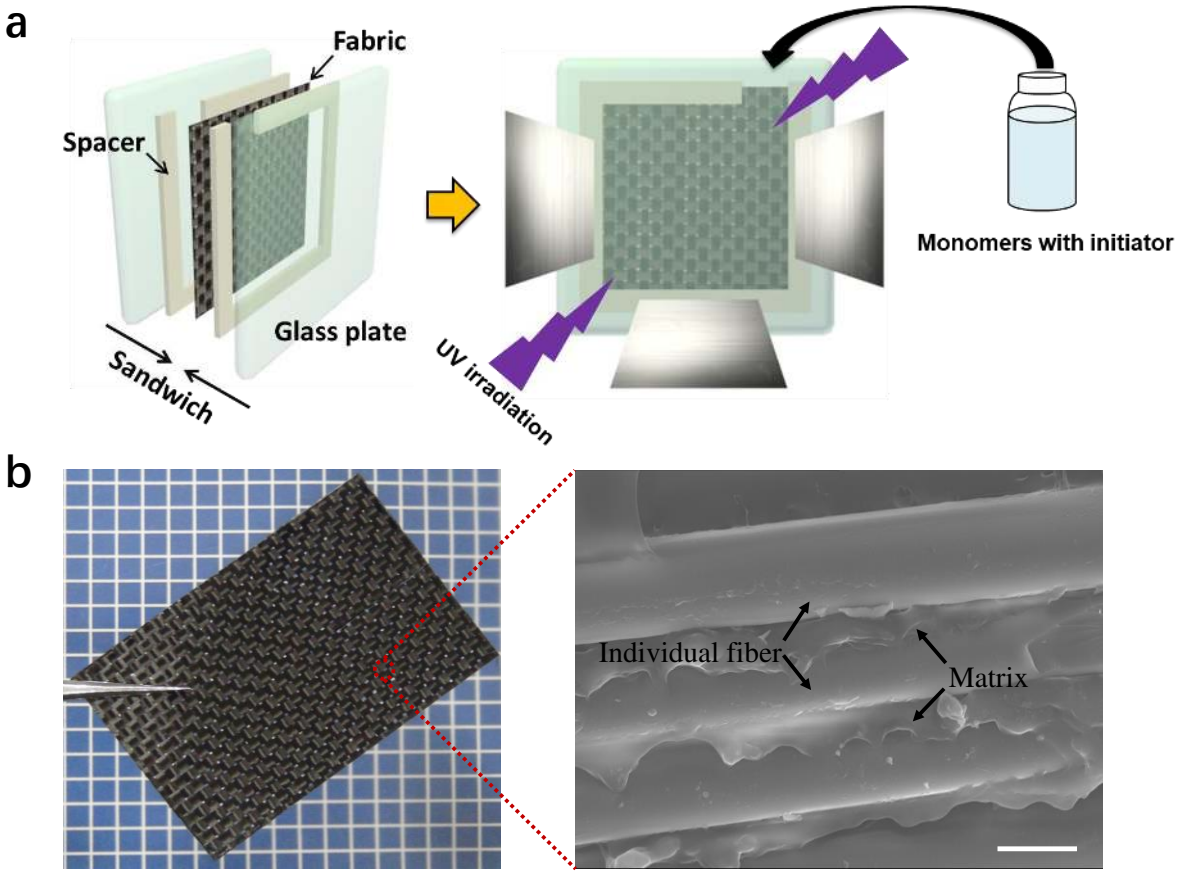

Figure S6. A typical procedure to prepare soft fiber-reinforced viscoelastomers. (a) Illustration of the preparation method. The low-viscosity monomers can easily permeate the fabric, leading to the formation of a strong interface and interlocking structure. (b) The appearance of the as-prepared soft FRP and enlarged view of the local area by SEM. The viscoelastomer matrix is M1-0.1. Individual fibers are fully wetted by the viscoelastomer matrix, suggesting a complete permeation of liquid monomers into fiber bundles and the formation of strongly bonded interface. The background grid size is 5 mm. The scale bar represents 5 μm.

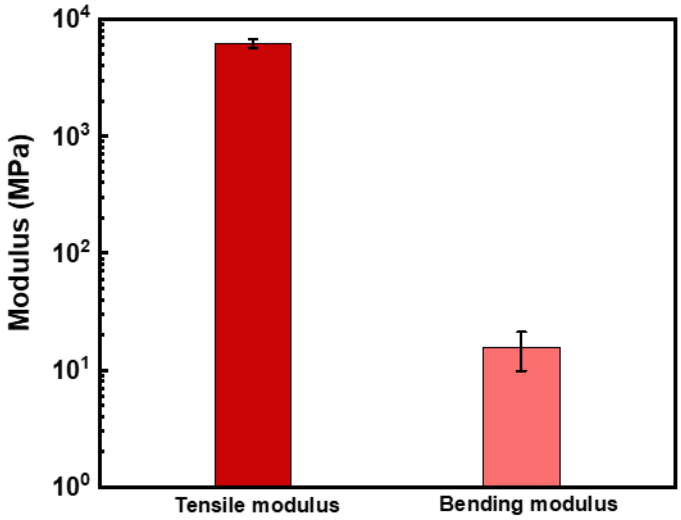

Figure S7. Anisotropy of soft fiber-reinforced polymer (FRP) from M1-0.1 and CF. The tensile modulus approaches 10 GPa while the bending modulus is about 10 MPa, indicating that the composite is highly stiff upon stretching but flexible under bending. The strain rates of tensile and bending tests were 0.07 mm min^{-1} and 0.042 mm min^{-1}, respectively. The velocity of tensile and bending tests were 50 mm min^{-1} and 30 mm min^{-1}, respectively.

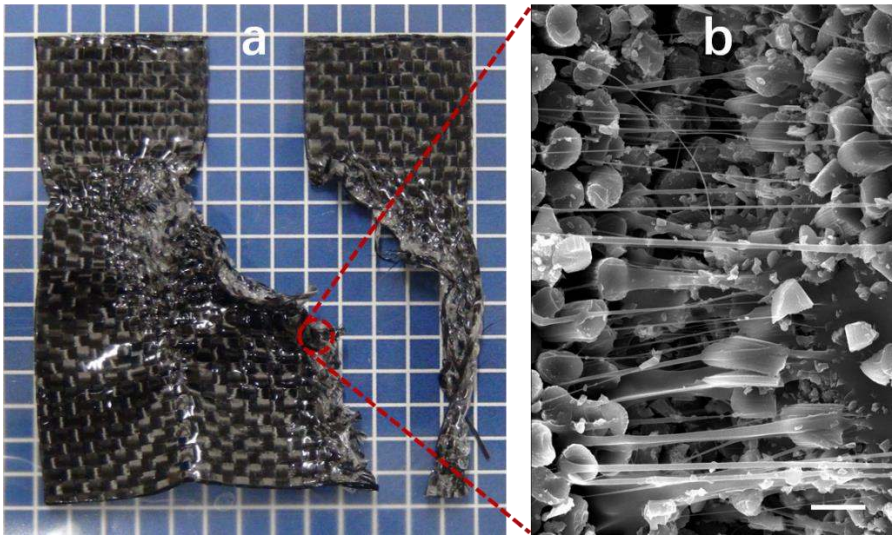

Figure S8. Photo and SEM images of the soft FRP (M1-0.1/CF) after tearing. (a) A large area of the composite is damaged. (b) Inside the damage zone, fibers are fractured and matrices are highly deformed or fractured. The background grid size in (a) is 5 mm. The scale bar in (b) represents 20 μm.

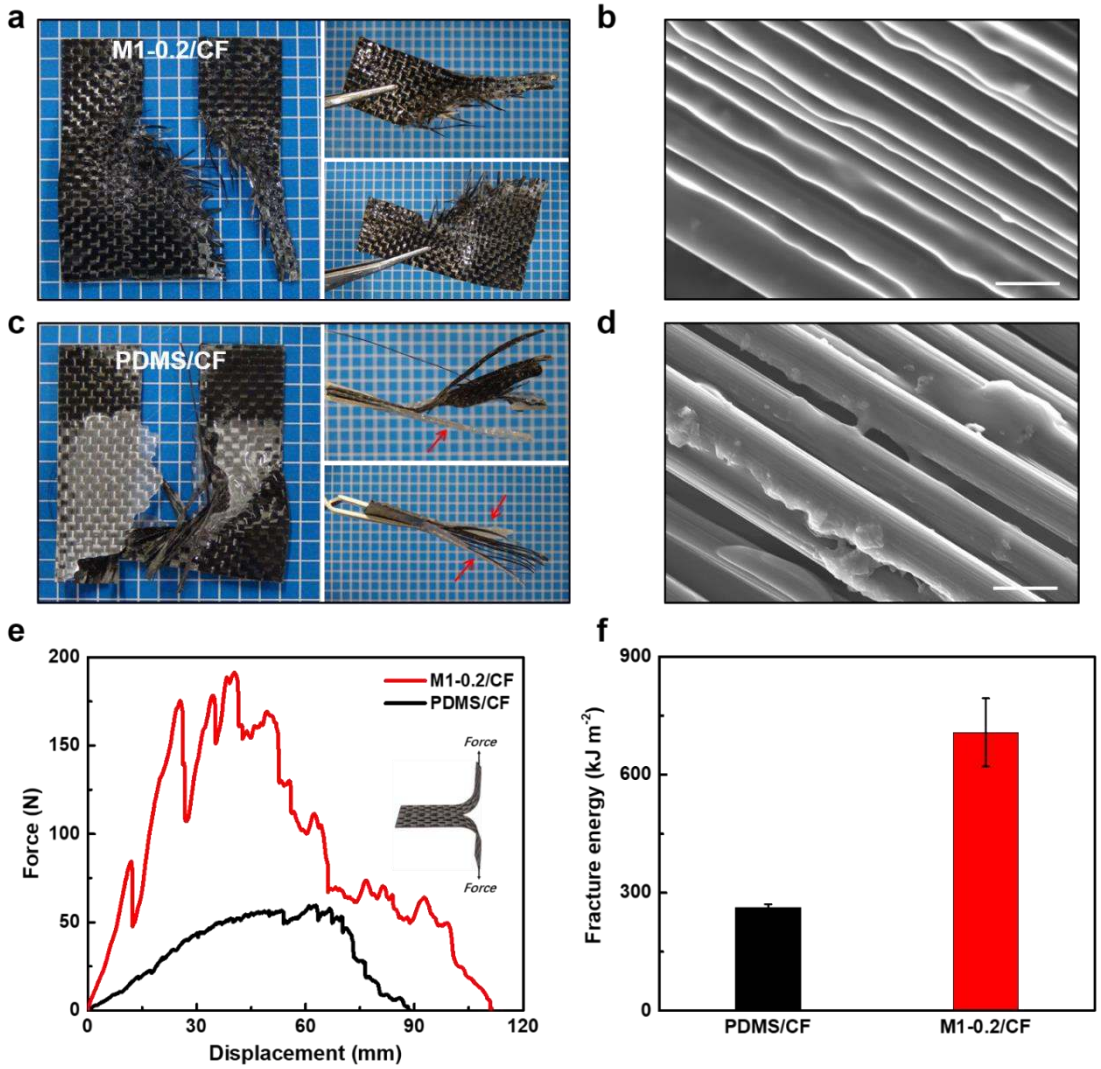

Figure S9. Comparison of tearing behaviors of soft FRPs fabricated from monomer solution of viscoelastomer M1-0.2 and from PDMS polymer. (a) The soft FRP prepared from viscoelastomer show no obvious interfacial debonding after tearing. (b) SEM observation suggests that individual fibers are strongly bonded by matrix. (c) Severe interfacial debonding occurs for the soft FRP prepared from PDMS polymer. (d) Voids exist among individual fibers, indicating that the polymer cannot permeate fiber bundles thoroughly. (e) Force-displacement curves of two kinds of soft FRPs. (f) Corresponding tearing energies of soft FRPs calculated from force-displacement curves. Soft FRP from the viscoelastomer possesses a toughness much higher than that of PDMS-based FRP. The results indicate that a strong interface is the premise to construct a tough soft FRP. Although the PDMS matrix is also soft and has a considerable energy dissipation density, the force cannot be transferred efficiently throughout the composite due to interfacial delamination. Sample width w = 40 mm, the background grid size in (a, c) is 5 mm. The scale bars in (b, d) represent 10 μm.

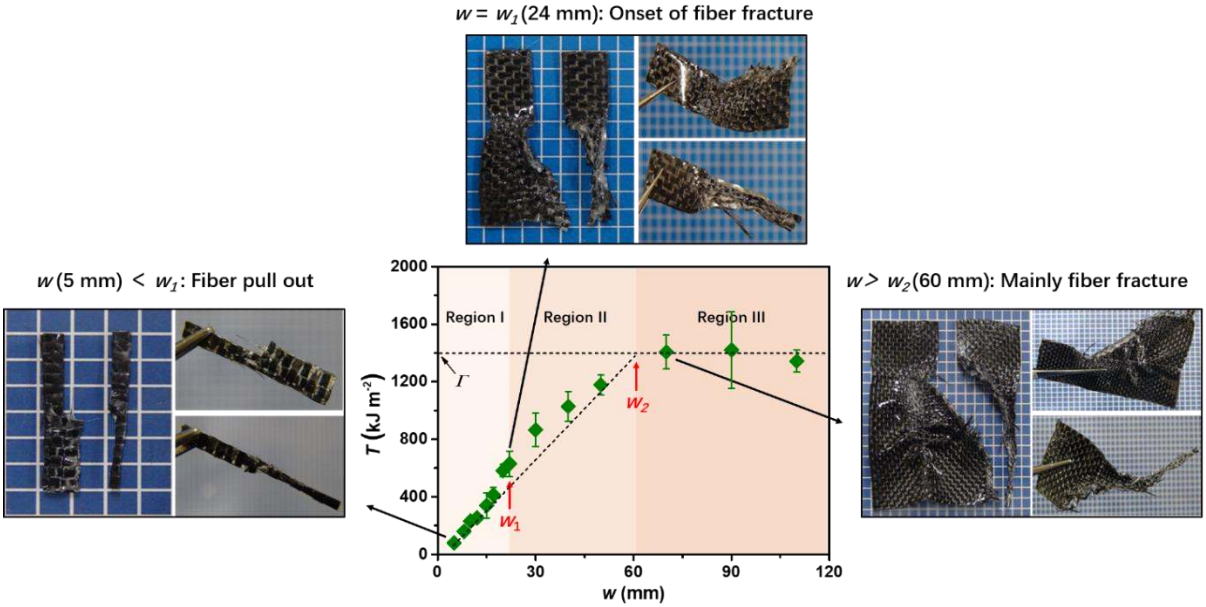

Figure S10. The plot of tearing energy *T* versus sample width *w*. The plot can be divided into three regions. The boundary of region I and II determines w_1, the onset width of fiber fracture. The boundary of Region II and III determines w_2, the onset width of saturation tearing energy, which reflects the size of energy dissipation zone. Here, M1-0.1/CF tested at 50 mm min^{-1} is taken as an example. The background grid size is 5 mm.

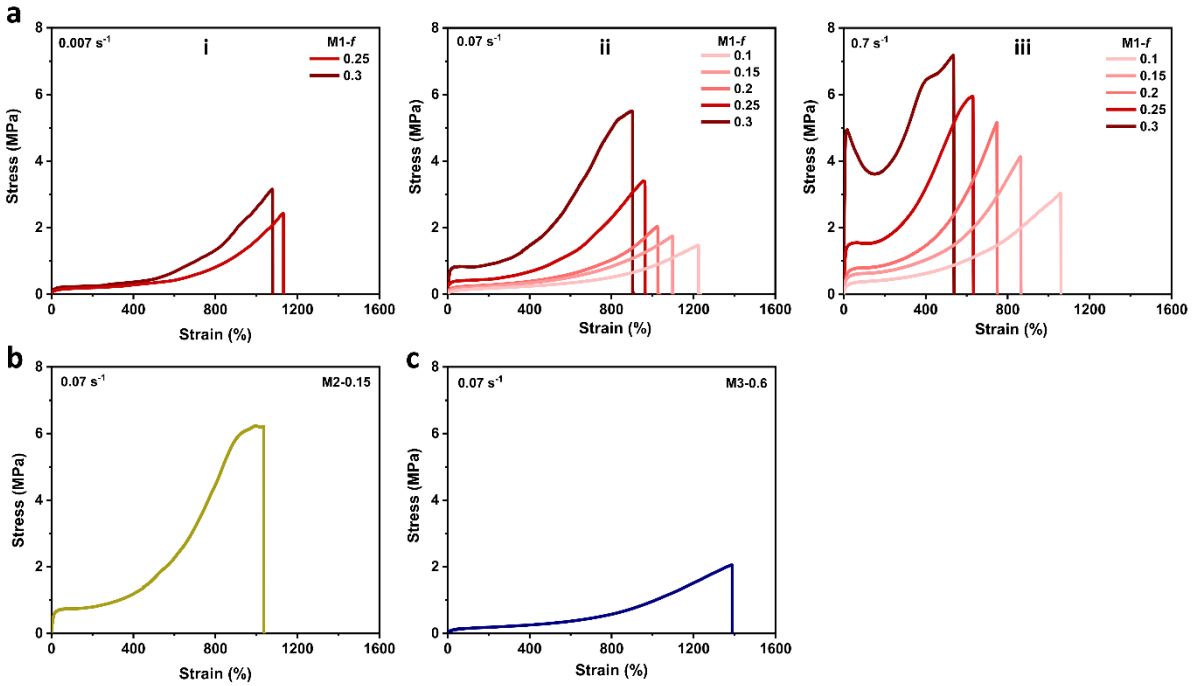

Figure S11. Strain rate dependence of viscoelastomer matrix M1-*f* and tensile properties of M2-0.15 and M3-0.6. (a) The matrices M1-*f* with different *f* are tested at strain rates of 0.007 s^{-1}, 0.07 s^{-1}, and 0.7 s^{-1} (Tensile velocities of 5 mm min^{-1}, 50 mm min^{-1}, and 500 mm min^{-1}) (a-i, a-ii, and a-iii), respectively. Results indicate that the tensile property of matrix is highly dependent on strain rate. Tensile modulus and failure stress of matrix increase with increasing strain rate, while tensile strain decreases. Both M1-0.3 and M1-0.25 show obvious yielding and relatively high tensile modulus of 105 MPa and 30 MPa at the strain rate of 0.7 s^{-1}, which behave similarly to thermal plastics. (b) Tensile property of M2-0.15. (c) Tensile property of M3-0.6.

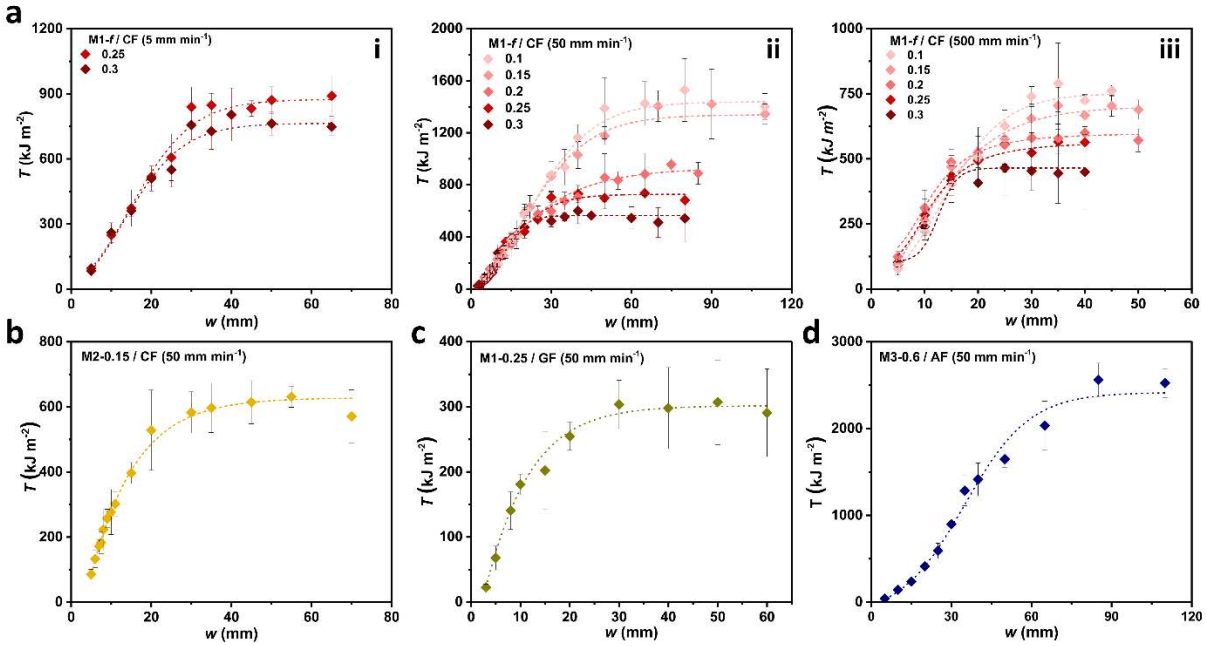

Figure S12. Sample size dependence of toughness as measured by tearing energy, *T*, for all composites fabricated in this work. (a) Tearing energy, *T*, as a function of sample width, *w*, for soft FRPs from M1-*f* and CF at testing velocities of 5 mm min^{-1} (i), 50 mm min-1 (ii), and 500 mm min^{-1} (iii), respectively. Since the elastomer matrices are viscoelastic, their mechanical behaviors are strain rate dependent (**Figure S11**). The inherent viscoelasticity of the matrices permits us to change mechanical behavior by changing the deformation rate. As expected, soft FRPs made from M1-*f* and CF show different w_2 and saturation *T* at different tearing velocities. (b) (c) (d) *T* as a function of *w* for soft FRPs from other combinations of matrix and fabrics. Two other series of viscoelastomers, P(BZA-co-IBA) and P(DEEA-co-IBA), denoted by M2-*f* and M3-*f*, respectively, are used in addition to M1-*f*. Also, glass fiber fabric (GF) and aramid fiber fabric (AF) are used in addition to CF. All fabrics have the same plain weave pattern to avoid difference in geometry. The results indicate that all composites show sample-size-dependent toughness. The saturation tearing energy is adopted as fracture energy *Γ*.

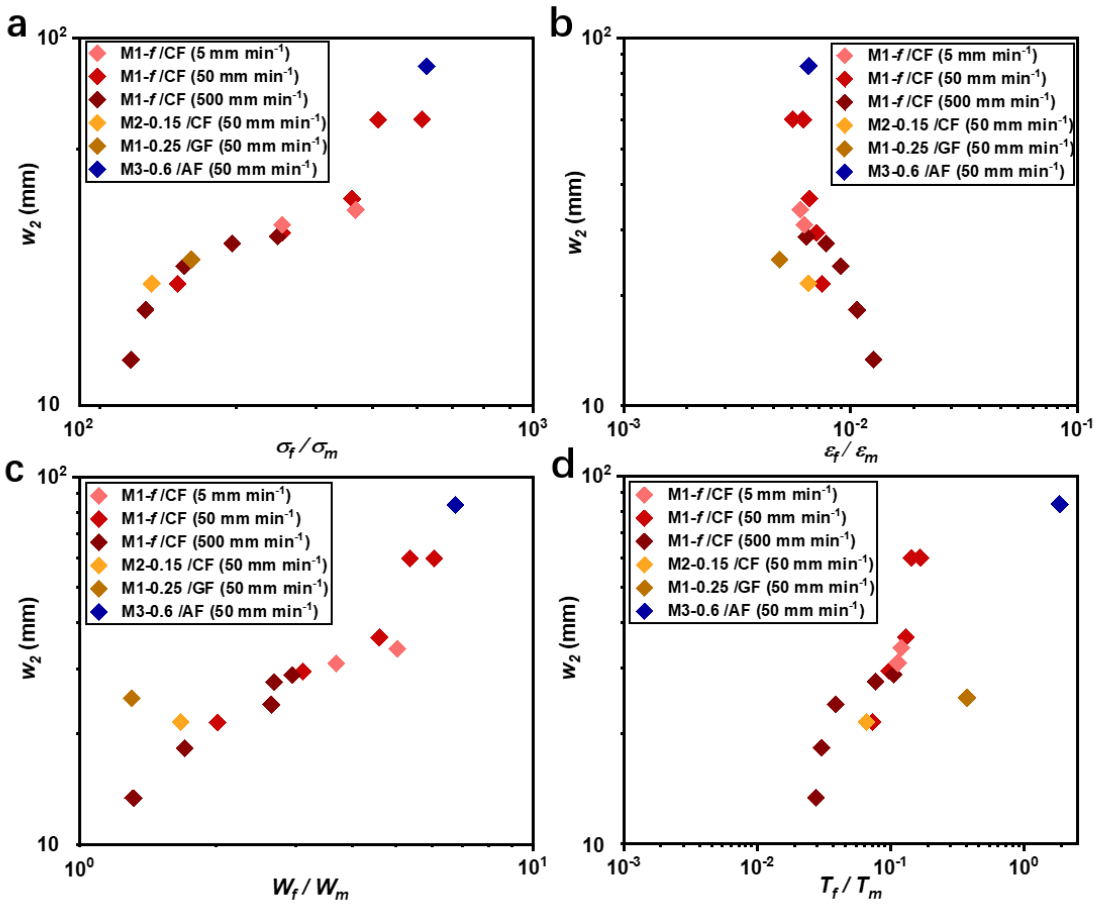

Figure S13. The relationship between w_2 and fiber/matrix property ratios for all soft FRPs in this work. (a) w_2 versus fiber/matrix fracture stress ratio, σ_f/σ_m; (b) w_2 versus fiber/matrix fracture strain ratio, $\varepsilon_f/\varepsilon_m$; (c) w_2 versus fiber/matrix work of extension ratio, W_f/W_m; (d) w_2 versus fabric/matrix tearing energy ratio, T_f/T_m.

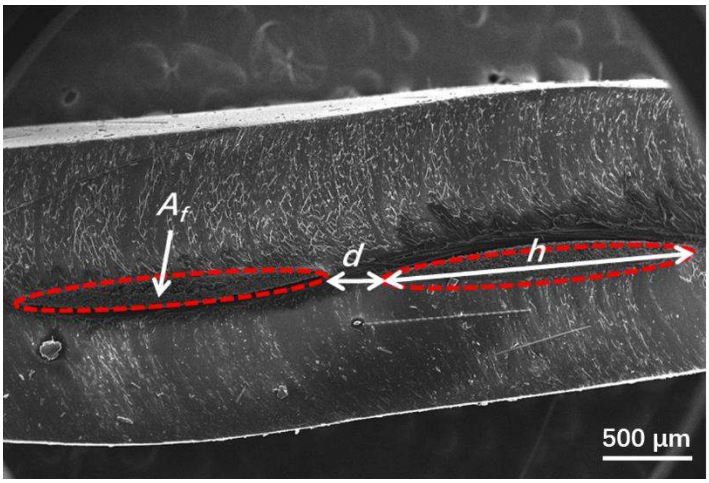

Figure S14. Geometry parameters used in the calculation of load transfer length in Appendix. A real composite M1-0.1/CF is taken as an example to illustrate geometry parameters. Cross-section SEM view of the composite shows the cross-sectional area of fiber bundles (area of red dotted circle) in the matrix, from which geometry parameters are estimated. The summarized geometry parameters of all fabrics in this work is shown in **Table S1**.

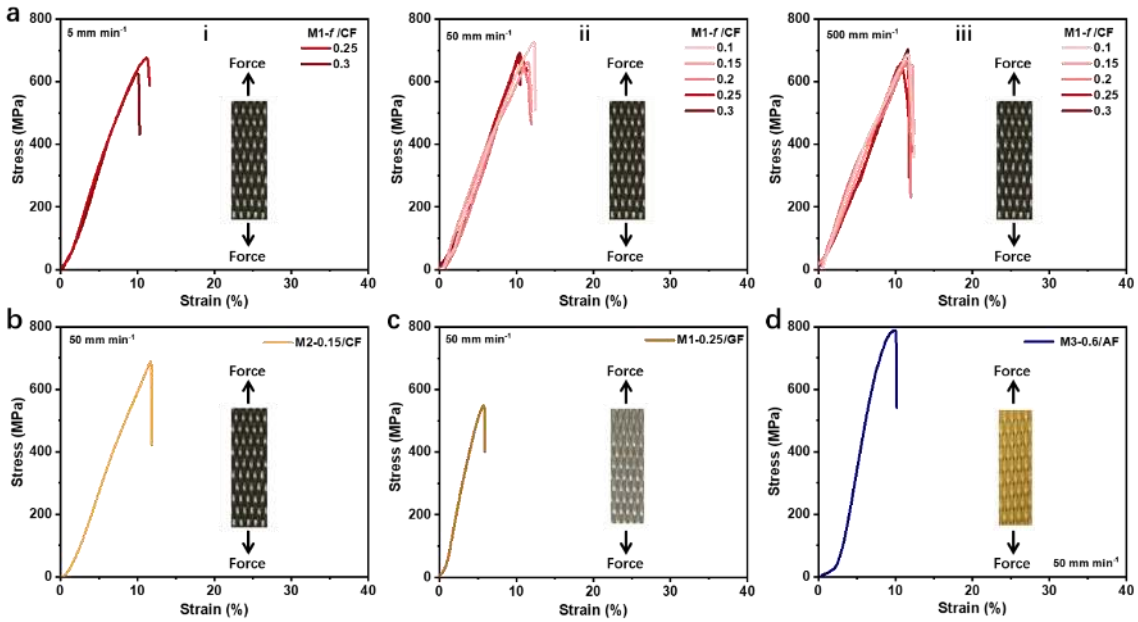

Figure S15. Tensile properties of soft FRPs using different combinations (a) The composites M1-*f* /CF with varied *f* are tested at tensile velocities of 5 mm min^{-1}, 50 mm min^{-1}, and 500 mm min^{-1} (a-i, a-ii, and a-iii), respectively. (b) Tensile property of M2-0.15/CF. (c) Tensile property of M1-0.25/GF. (d) Tensile property of M3-0.6/AF. Sample width and gauge length are 10 mm and 20 mm, respectively.

Table S1. Structural parameters of the three plain weave fiber fabrics used in this work. Parameters include fabric area density (ρ_a), fabric thickness (t), cross-sectional perimeter of a fiber bundle (S), cross-sectional area of a fiber bundle (A_f), effective distance between adjacent fiber bundles (d), width of a fiber bundle (h), single fiber radius (r).

Fabrics	ρ_a (g m^{-2})	t (mm)	S [a)] (mm)	A_f [a)] (mm^2)	d [a)] (mm)	h [a)] (mm)	r (μm)
CF	200	0.30	3.8	0.204	0.361	1.705	5
GF	590	0.59	4.5	0.403	0.216	2.048	7
AF	320	0.55	4.2	0.396	0.184	1.812	8

a) These parameters were estimated from the SEM images of the corresponding composites.

Table S2. Summary of mechanical properties of fabrics and corresponding fiber bundles. The properties include tensile fracture force (F_f) and nominal stress (σ_f), fracture strain (ε_f), Young's modulus (E_f), work of extension (W_f), and tearing energy (T_f). Each sample was tested $N \geqslant 3$ times to obtain the average value. The testing velocity was 50 mm min^{-1}.

Sample code	F_f [a)](N)	σ_f(MPa)	ε_f(%)	E_f(GPa)	W_f(MJ m^{-3})	T_f(kJ m^{-2})
CF fabric	744 ± 54	496 ± 23	8.8 ± 0.2	6.6 ± 0.3	20.3 ± 3.8	2.5 ± 0.2
CF fiber bundle	183 ± 32	895 ± 41	6.8 ± 0.1	21.8 ± 1.6	39.0 ± 4.2	—
GF fabric[b)]	1210 ± 67	410 ± 22	5.7 ± 0.6	7.4 ± 1.0	14.3 ± 1.5	10.2 ± 1.1
GF fiber bundle[b)]	228 ± 16	565 ± 40	4.7 ± 0.4	17.7 ± 0.7	16.4 ± 2.1	—
AF fabric	1774 ± 85	645 ± 31	10.6 ± 0.4	7.8 ± 1.3	37.0 ± 2.3	17.0 ± 1.0
AF fiber bundle	430 ± 23	1085 ± 58	9.1 ± 0.3	17.3 ± 1.4	55.8 ± 3.4	—

a) Fabric is in a rectangle shape with a width of 5 mm.

b) Data of soaked GF sample in **Figure S2** is employed.

Table S3. Basic physicochemical properties of monomers used in this work.[10] The η, ΔT_b, and ρ are viscosity, boiling point, and density of the monomers, respectively.

Monomers	η (mPa · s)	ΔT_b at 760 mm Hg (°C)	ρ (g cm^{-3})
PEA	8.7	290	1.102-1.110
BZA	2.2	248	1.057-1.063
DEEA	2.9	240	1.014-1.020
IBA	7.7	246	0.990-0.996

Table S4. Glass transition temperature (T_g) of homopolymers and copolymers used in this work.

Sample	f	T_g (°C)
Poly(PEA)	-	10
Poly(BZA)	-	11
Poly(DEEA)	-	-57
Poly(IBA)	-	74
Poly(PEA-co-IBA) (M1-*f*)	0.1	15
	0.15	16
	0.2	18
	0.25	19
	0.3	22
Poly(BZA-co-IBA) (M2-*f*)	0.15	20
Poly(DEEA-co-IBA) (M3-*f*)	0.6	5

Table S5. Summary of mechanical properties of the viscoelastomer matrices at different testing velocities. The mechanical properties are tensile fracture stress (σ_m), fracture strain (ε_m), Young's modulus (E_m), work of extension (W_m), and tearing energy (T_m). Each sample was tested $N \geqslant 3$ times to obtain the average value. The shear modulus μ_m of the matrix is 1/3 of the Young's modulus. The mechanical tests were performed at room temperature (24 °C).

Sample code	Testing velocity (mm min^{-1})	Strain rate (s^{-1})	f	σ_m (MPa)	ε_m (%)	E_m (MPa)	W_m (MJ m^{-3})	T_m (kJ m^{-2})
M1-f	5	0.7	0.25	2.20 ± 0.28	1133 ± 24	1.71 ± 0.15	7.76 ± 0.28	20.66 ± 1.26
			0.3	3.20 ± 0.06	1082 ± 25	2.07 ± 0.23	10.57 ± 0.59	21.91 ± 1.55
	50	0.07	0.1	1.57 ± 0.08	1225 ± 6.4	0.80 ± 0.03	6.43 ± 0.16	14.84 ± 1.22
			0.15	1.96 ± 0.45	1101 ± 16	0.84 ± 0.07	7.27 ± 0.74	17.26 ± 4.92
			0.2	2.24 ± 0.23	1030 ± 18	1.72 ± 0.30	8.49 ± 0.93	19.03 ± 1.68
			0.25	3.20 ± 0.16	961 ± 45	2.23 ± 0.49	12.55 ± 3.81	25.39 ± 1.16
			0.3	5.44 ± 0.18	905 ± 40	4.39 ± 0.61	19.34 ± 2.15	33.96 ± 3.65
	500	0.007	0.1	3.27 ± 0.34	1063 ± 37	2.58 ± 0.28	13.22 ± 1.80	23.48 ± 1.38
			0.15	4.11 ± 0.64	868 ± 24	3.51 ± 0.88	14.52 ± 1.28	32.06 ± 1.83
			0.2	5.26 ± 0.32	752 ± 12	4.64 ± 1.21	14.72 ± 0.45	63.79 ± 1.27
			0.25	6.40 ± 0.02	634 ± 60	30.45 ± 4.21	22.80 ± 1.22	81.77 ± 3.80
			0.3	6.89 ± 0.42	538 ± 30	105.31 ± 11.58	29.65 ± 0.99	89.69 ± 9.44
M2-f	50	0.07	0.15	6.20 ± 0.04	1041 ± 56	3.96 ± 0.56	23.34 ± 2.74	37.65 ± 0.88
M3-f	50	0.07	0.6	1.86 ± 0.25	1391 ± 18	0.34 ± 0.05	8.29 ± 1.84	9.18 ± 1.00

Table S6. Summary of relevant ratios of fiber/matrix mechanical properties and experimentally observed force transfer length w_2 for different composite systems. The ratios include tensile fracture stress ratio (σ_f/σ_m), fracture strain ratio ($\varepsilon_f/\varepsilon_m$), Young's modulus /shear modulus ratio (E_f/μ_m), work of extension ratio (W_f/W_m), and tearing energy ratio (T_f/T_m). For comparison, the theoretical force transfer length l_T for a model composite consisting of parallel fibers embedded in a soft matrix is calculated from **Equation S2** using the structure parameters of fabrics shown in **Table S1** and the fiber/matrix modulus ratio of the composites.

Sample code	Testing velocity (mm min^{-1})	f	σ_f/σ_m ($\times10^2$)	$\varepsilon_f/\varepsilon_m$ ($\times10^{-3}$)	E_f/μ_m ($\times10^4$)	W_f/W_m	T_f/T_m ($\times10^{-2}$)	w_2 (mm)	l_T (mm)
M1-*f*/CF	5	0.25	4.07	6.00	3.75	5.03	12.00	34.10	40.26
		0.3	2.80	6.28	3.11	3.69	11.32	31.06	36.62
	50	0.1	5.70	5.55	7.99	6.07	5.12	60.03	58.73
		0.15	4.57	6.18	7.64	5.36	14.37	59.94	57.45
		0.2	4.00	6.60	3.73	4.59	13.03	36.53	40.13
		0.25	2.80	7.08	2.87	3.11	9.77	29.53	35.23
		0.3	1.65	7.51	1.46	2.02	7.30	21.43	25.11
	500	0.1	2.74	6.40	2.49	2.95	10.56	28.85	32.78
		0.15	2.18	7.83	1.83	2.69	7.74	27.62	28.10
		0.2	1.70	9.04	1.38	2.65	3.89	23.97	24.45
		0.25	1.40	10.73	0.21	1.71	3.03	18.26	9.54
		0.3	1.30	12.64	0.06	1.32	2.77	13.35	5.13
M2-*f*/CF	50	0.15	1.44	6.53	1.62	1.67	6.59	21.50	26.46
M1-*f*/GF	50	0.25	1.77	4.89	2.38	1.31	40.17	24.02	31.83
M3-*f*/AF	50	0.6	5.83	6.54	15.04	6.74	184.78	83.86	77.77

Table S7. Summary of mechanical properties of varied composites at different testing velocities. The properties include tensile fracture stress (σ_c), fracture strain (ε_c), Young's modulus (E_c), tensile work of extension to fracture the composites (W_c), the volume weighed average of the work of extension of the fiber bundle and the matrix at fracture (W_{eff}), and tearing energy (T_c). Each sample was tested $N \geqslant 3$ times to obtain the average value. Sample width and gauge length for tensile test are 10 mm and 20 mm, respectively.

Sample code	Testing velocity (mm min^{-1})	f	σ_c (MPa)	ε_c (%)	E_c (MPa)	W_c (MJ m^{-3})	W_{eff} (MJ m^{-3})	T_c (kJ m^{-2})
M1-f/CF	5	0.25	667 ± 58	11.06 ± 0.93	6.67 ± 0.71	40.49 ± 2.97	23.36 ± 2.26	856 ± 24
		0.3	618 ± 45	10.45 ±1.28	6.52 ± 0.35	34.75 ± 3.61	24.77 ± 2.42	760 ± 28
	50	0.1	730 ± 65	12.36 ± 0.88	6.43 ± 0.50	44.18 ± 3.15	22.70 ± 2.20	1390 ± 41
		0.15	652 ± 59	11.86 ± 0.43	6.23 ± 1.11	42.23 ±1.92	23.12 ± 2.49	1435 ± 64
		0.2	645 ± 31	11.81 ± 1.33	6.72 ± 0.47	37.74 ± 3.62	23.73 ± 2.59	883 ± 46
		0.25	678 ± 56	11.26 ± 1.62	6.57 ± 0.41	39.83 ± 3.73	26.76 ± 4.03	712 ± 26
		0.3	691 ± 67	10.52 ± 0.9	6.51 ± 0.62	35.28 ± 2.01	29.15 ± 3.20	548 ± 29
	500	0.1	687 ± 55	12.15 ± 0.58	6.66 ± 0.26	46.37 ± 4.15	26.09 ± 3.02	750 ± 34
		0.15	665 ± 60	12.26 ± 0.73	6.36 ± 0.30	45.48 ± 2.88	26.74 ± 2.76	682 ± 25
		0.2	654 ± 49	11.91 ± 1.21	6.92 ± 0.69	40.63 ± 3.29	26.84 ± 2.35	576 ± 15
		0.25	662 ± 31	11.66 ± 1.53	6.44 ± 1.37	40.82 ± 3.82	30.89 ± 2.73	552 ± 20
		0.3	692 ± 41	11.71 ± 1.46	6.57 ± 0.87	43.66 ± 3.24	34.31 ± 2.62	453 ± 9
M2-f/CF	50	0.15	688 ± 65	12.04 ± 0.77	6.85 ± 0.39	38.37 ± 3.96	30.04 ± 2.38	597 ± 24
M1-f/GF	50	0.25	515 ± 33	6.12 ± 0.51	7.24 ± 1.22	19.76 ± 3.10	15.46 ± 2.58	300 ± 7
M3-f/AF	50	0.6	771 ± 56	11.27 ± 1.83	7.88 ± 1.70	37.50 ± 2.03	32.02 ± 0.92	2543 ± 26

Table S8. Summary of mechanical properties of materials shown in Figure 4 in the manuscript. The mechanical properties are tensile modulus (E), tensile strength (σ), fracture energy (Γ), density (ρ), specific strength (σ/ρ), specific fracture energy (Γ/ρ).

Material	E (GPa)	σ (MPa)	Γ (kJ m^{-2})	ρ (g cm^{-3})	σ/ρ (Pa g^{-1} m^3)	Γ/ρ (J g^{-1} m)
Viscoelastomer/fiber[this work]	5.2-7.9	480-770	300-2500	0.9-1.2	310-670	0.3-2.4
PA gel/fiber[1-3]	5.0-7.6	240-340	400-1000	≈1.0	240-340	0.4-1.0
PDMS or Rubber/fiber[this work]	4.8-7.2	400-720	90-260	1.0-1.4	260-500	0.06-0.2
CFRP and GFRP[11-14]	12.9-162	98-1275	0.36-20	1.4-2.0	50-860	4.3×10^{-4}-1.1×10^{-2}
Metals and alloys[14, 15]	16.6-346	18-1525	0.6-190	1.6-22	0.9-200	9.4×10^{-5}-8.6×10^{-3}
Metallic glasses[16-18]	30.3-137	660-1800	0.003-340	3.9-8.3	100-294	1.8×10^{-5}-1.2×10^{-2}
Ceramics[19, 20]	7.0-545	5-1970	0.02-0.05	1.7-4.0	0.5-620	1.0×10^{-6}-1.3×10^{-4}
Engineering polymers and elastomers[21]	0.3-4.1	0.2-104	0.3-29.7	0.9-1.4	0.7-80	5.3×10^{-5}-2.4×10^{-2}
Woods[14]	6.8-17.1	31-60	2.4-5.9	0.6-0.8	45-85	3.2×10^{-3}-9.2×10^{-3}

References

[1] D. R. King, T. L. Sun, Y. Huang, T. Kurokawa, T. Nonoyama, A. J. Crosby, J. P. Gong, *Mater. Horiz.* **2015**, *2*, 584.

[2] Y. Huang, D. R. King, T. L. Sun, T. Nonoyama, T. Kurokawa, T. Nakajima, J. P. Gong, *Adv. Funct. Mater.* **2017**, *27*, 1605350.

[3] Y. Huang, D. R. King, W. Cui, T. L. Sun, H. Guo, T. Kurokawa, H. R. Brown, C.-Y. Hui, J. P. Gong, *J. Mater. Chem. A* **2019**, *7*, 13431.

[4] J.M. Hedgepeth, *NASA TN D-882* **1961**.

[5] H.L. Cox, *Br. J. Appl. Phys.* **1952**, *3*, 72.

[6] C.Y. Hui, Z. Liu, S.L. Phoenix, *Extreme Mech. Lett.* **2019**, *33*, 100573.

[7] A. N. Gent, G. S. Fielding-Russell, D. I. Livingston, D. W. Nicholson, *J. Mater. Sci.* **1981**, *16*, 949.

[8] A. N. Gent, G. L. Liu, *J. Mater. Sci.* **1991**, *26*, 2467.

[9] L. Chen, T. L. Sun, K. Cui, D. R. King, T. Kurokawa, Y. SARUWATARI, J. P. Gong, *J. Mater. Chem. A* **2019**, *7*, 17334.

[10] Chemical book, https://www.chemicalbook.com/CASDetailList_29600_EN.htm.

[11] W.F. Thomas, *Nature* **1973**, *242*, 455.

[12] J. McLoughlin, *Nature* **1970**, *227*, 701.

[13] H. Ku, H. Wang, N. Pattarachaiyakoop, M. Trada, *Compos. Part B-Eng.* **2011**, *42*, 856.

[14] M.F. Ashby, *MRS Bull.* **2005**, *30*, 994.

[15] B. Gludovatz, A. Hohenwarter, D. Catoor, E.H. Chang, E.P. George, R.O. Ritchie, *Science* **2014**, *345*, 1153.

[16] L.-B. Mao, H.-L. Gao, H.-B. Yao, L. Liu, H. Cölfen, G. Liu, S.-M. Chen, S.-K. Li, Y.-X. Yan, Y.-Y. Liu, S.-H. Yu, *Science* **2016**, *354*, 107.

[17] R.O. Ritchie, *Nat. Mater.* **2011**, *10*, 817.

[18] J. Schroers, W.L. Johnson, *Phys. Rev. Lett.* **2004**, *93*, 255506.

[19] E. Munch, M.E. Launey, D.H. Alsem, E. Saiz, A.P. Tomsia, R.O. Ritchie, *Science* **2008**, *322*, 1516.

[20] W. Clegg, K. Kendall, N.M. Alford, T. Button, J. Birchall, *Nature* **1990**, *347*, 455.

[21] Á. Kmetty, T. Bárány, J. Karger-Kocsis, *Prog. Polym. Sci.* **2010**, *35*, 1288.